Bachelor's Thesis in Physics

Evaluating the Implementation of Neutrino Interaction Simulations with the GiBUU Software Package in the KM3NeT Simulation-Chain

Submitted by
Hannes Warnhofer
August 26, 2022

Erlangen Centre for Astroparticle Physics
Friedrich-Alexander-Universität Erlangen-Nürnberg

Supervisor: Prof. Dr. Uli Katz

Contents

1 Introduction and Motivation

Since Wolfgang Pauli postulated the existence of an elementary particle with neutral electrical charge that hardly interacts with matter in 1930, the nature of neutrinos and their appearance in the context of the Standard Model of Particle Physics has been an extensive subject of study. Through the evolution of experiments the measurement of neutrinos in different energy ranges became possible, which lead to a number of important discoveries. The study of neutrino oscillations has lead to the conclusion, that neutrinos are not massless, in contrary to their description in the Standard Model and the ongoing analysis of this effect is aimed at a deeper understanding of these masses. This is one of the examples highlighting that the study of neutrinos is an important field of physics, testing the limits of the Standard Model and exploring possible new physics.

One detection approach is the usage of water Cherenkov telescopes that measures the Cherenkov radiation produced by particles that are generated in neutrino-nucleus interactions and are then propagating through water for the determination of the initial neutrino's type, energy and momentum. An important part in the analysis chain of such a telescope is the simulation of the neutrino-nucleus interaction, for which a number of different models are existent and used in the field of high energy particle physics.

Currently, an underwater Cherenkov neutrino telescope is being built in the Mediterranean Sea by the KM3NeT collaboration, with one part of this telescope being dedicated to the study of neutrino oscillations and the determination of the neutrino mass hierarchy. The analysis chain is currently relying on the GENIE neutrino event generator, that is implemented into KM3NeT via the gSeaGen software package.

This work is aimed at the analysis of another event generator called GiBUU, which has a different approach regarding the simulation of final state interactions during the scattering processes of neutrinos on nuclei, that possibly enables a more detailed measurement in the future. Another important aspect is the comparison of different event generators to gain knowledge about systematic uncertainties originating from the event generation. The implementation of GiBUU into the KM3NeT chain with the KM3BUU package will be analysed and compared to the gSeaGen chain. The goal is to create a basis for both further development and the general usage of the KM3BUU package, as well as giving a first insight into the working mechanism of GiBUU with the KM3NeT simulation chain.

2 Fundamental Knowledge

In the first part of this work, an overview about the physical basics that are needed to understand the ongoing analysis are given. Furthermore the principle behind the KM3NeT neutrino telescope will be explained and the methods of operation of the two neutrino-nucleus interaction simulators GiBUU and gSeaGen and their role in the KM3NeT simulation chain will be outlined.

2.1 Physical Basics

First of all, the physical basics behind neutrino-nucleus interactions will be explained. In addition to that, a short insight on the physics of neutrino oscillations and the role of measuring this oscillation in the process of determining the neutrino mass hierarchy - which is one of the main investigation fields of KM3NeT - will be given.

NOTE: The following two subsections will be giving a more or less basic overview about the description of particle physics with the Standard Model, with subsection 2.1.2 being focused on neutrinos and the weak interaction. Those sections are thought for everyone who is not familiar with this subject. The readers who are not new to particle physics and don't need a short revision can simply skip this part and jump straight to subsection 2.1.3 on page 12, where neutrinos-nucleus interactions will be presented in more detail.

2.1.1 The Standard Model of Particle Physics

This section aims to give a short introduction into the world of particle physics and an overview about the particles and forces described in the Standard Model of Particle Physics. Covering all principles behind the analysis of neutrinos and neutrino oscillations is way beyond the scope of this work, but nevertheless an overview about the current theory will be given, in order to be able to place the analysis of neutrino oscillations in the general context of particle physics and the development of the Standard Model.

Introduction to Particle Physics

Generally, in all fields of physics, one can break down everything into two basic observations, that go along with the common experience about the world we are living in (Mann, 2010):

- Matter exists (there are things)
- Interactions occur (things are happening)

In particle physics, the understanding of these two observations is tried to be reduced to a level, that is as elementary as possible. This means, that the main goal of particle physics is to find and characterize the smallest particles, that can be treated as some sort of individual objects and to be able to describe the principles and consequences of their interactions. In contrary to most other subdisciplines of physics, the laws and components occurring in these interactions were or are not known and one can not derive the behaviour of all the involved actors from known theories. The study of particle physics is a strongly interwoven interplay between high energy collision experiments,

detector physics, the analysis of cosmological data, statistical analysis of huge amounts of data, model building and numerical computation and simulations. Step by step, this allows to propose several assumptions about the involved particles, their interactions and basic symmetries, that are respected by them. With these models one should be able to make falsifiable predictions about the behavior of the involved objects, which can be tested by corresponding experiments and therefore allow to favor one model over another (Mann, 2010).

On the basis of this approach, the so called *Standard Model of Particle Physics* (or often simply *Standard Model*) was developed. It is one of the most successful - nevertheless incomplete - theories in physics and is able to describe the "fundamental interactions between elementary particles" with astonishing precision (Woithe, Wiener, and Veken, 2017).

The Fundamental Forces

The current understanding of particle physics is, that there are four fundamental forces, which act on the elementary particles, that form the matter in our universe: *Gravity*, the *electromagnetic force*, the *strong force* and the *weak force*. Here a major flaw of the Standard Model theory shows up, as it fails to describe gravity in the context of elementary particles (Griffiths, 2008).

The electromagnetic force acts upon particles according to their *electrical charge*, which is commonly known from experiences in daily life. The other two forces described in the Standard Model, appear on much smaller scales than electromagnetism (and gravity) and we are therefore way less familiar with their origins and behaviours from our daily experiences. Both of them act upon particles according to properties comparable to the electric charge in the interaction with the electromagnetic force. One says, that these forces are coupling to the corresponding property.

The weak force is responsible for certain types of radioactive decays and the interaction depends on the so called *flavour* (or also weak charge) of a particle (Robinson et al., 2008). The electromagnetic force and the weak force can be seen as two parts of the same theory, called the electroweak theory. At high enough energies the difference between both forces becomes negligible and they act together as the electroweak force.

The strong force is connected with the formation of protons and neutrons and their attracting potential inside the nucleus. The property related to the strong interaction is the so called *color* (or also strong charge) (Mann, 2010). In table 2.1 an overview about the four known forces is given, where the strength of each force is given in relation to that of the strong force. Note that there are already some mediator particles with their masses given. This will be explained later on in this subsection.

You can see, that gravity is far less powerful than the other three forces, but due to their long-scale range, gravity and electromagnetism are the forces we mainly experience in daily life.

Leptons

When looking at the elementary particles, meaning particles that have no known constituents, one can find that there are three different kinds of particles: *Leptons*, *quarks* and interaction particles, so called *gauge bosons*, that are responsible for mediating the fundamental forces. All known matter is made of *fermions* (leptons and quarks), which can be organized into three generations, with each generation containing heavier and more unstable particles. The particles from higher generations

	Gravity	Electromagnetism	Weak Force	Strong Force
Example	Planetary motion	Motion of an electron	Radioactive decay	Formation of a proton
Range	Long	Long	Short	Short
Strength	10^{-40}	10^{-2}	10^{-5}	1
Mediator	Graviton *(hypothetical)*	Photon	W^+,W^-,Z^0	Gluons
Mass	(0)	0	$\approx 10^2\,\mathrm{GeV/c^2}$	0

Table 2.1: An overview about the four fundamental forces (Mann, 2010) and (Povh et al., 2014)

quickly decay into the more stable ones, which is why all the stable matter in the universe is made up from those first generation particles (Griffiths, 2008).

Leptons are characterized by their flavor and electromagnetic charge. They don't have a colour, so they don't interact with the strong force, but only with electromagnetism and the weak force (and gravity). Besides the flavor, one could also characterize them using the electromagnetic charge, the electron number, muon number and tau number. In table 2.2 these characteristics of the leptons are summarized together with their (estimated) masses (Mann, 2010).

Generation	Flavor	EM Charge q	electron number l_e	muon number l_μ	tau number l_τ	Mass m in MeV
First	electron e	-1	1	0	0	0.511
	e-neutrino ν_e	0	1	0	0	$< 2 \times 10^{-6}$
Second	muon μ	-1	0	1	0	106
	μ-neutrino ν_μ	0	0	1	0	< 0.19
Third	tau τ	-1	0	0	1	1777
	τ-neutrino ν_τ	0	0	0	1	< 18

Table 2.2: Basic properties of leptons (Griffiths, 2008) and (Mann, 2010)

You can see that flavor is the property, which is often used for distinguishing different types of particles. To each of the shown particles exists an antiparticle, which has the same mass, but reversed electromagnetic charge and electron-, tau- and muon-number, which adds up to a total of 12 known different leptons (Griffiths, 2008).

Quarks

Leptons are not interacting with the strong force because they are color neutral (they don't have a strong charge). Quarks on the other hand are experiencing the strong force and each quark flavor comes in three colors: Red (R), blue (B) and green (G). A strong interaction has the effect of changing a quark of one color (e.g. red) into a quark of another color (e.g. blue). Likewise, a weak interaction changes a lepton or quark of one flavor into a lepton or quark of another flavor in the same generation, e.g. an electron to its corresponding neutrino (Mann, 2010). In table 2.3

the characteristics of the quarks are summarized analogous to table 2.2. One can assign similar properties like electron, tau and muon number to the quarks, connected with their flavor. The flavors can be characterized using the quantum numbers strangeness s, charm c, bottomness (also: beauty) b and topness (also: truth) t and their electric charge. For consistency, we could also use the terms upness u and downness d, even if those are redundant when the other numbers are given and are not commonly used (Griffiths, 2008). This is shown in table 2.4.

Generation	Flavor	EM Charge q	Color	Mass m in MeV
First	up u	$+2/3$	(R,G,B)	2
	down d	-1/3	(R,G,B)	5
Second	charm c	$+2/3$	(R,G,B)	1200
	strange s	-1/3	(R,G,B)	100
Third	top t	$+2/3$	(R,G,B)	$171,000$
	bottom b	-1/3	(R,G,B)	$4,200$

Table 2.3: Basic properties of quarks (Mann, 2010)

Generation	Flavor	q	d	u	s	c	b	t
First	up u	$+2/3$	-1	0	0	0	0	0
	down d	-1/3	0	1	0	0	0	0
Second	charm c	$+2/3$	0	0	-1	0	0	0
	strange s	-1/3	0	0	0	1	0	0
Third	top t	$+2/3$	0	0	0	0	-1	0
	bottom b	-1/3	0	0	0	0	0	1

Table 2.4: Classification of quarks (Griffiths, 2008)

Like it is the case with leptons, for each quark flavor there exists an antiquark with the same mass reversed electrical charge q and reversed quantum numbers (in this case d, u, s, c, b and t). The antiquarks have the strong charges (or colors) antired $\bar{R}$, antiblue $\bar{B}$ and antigreen $\bar{G}$. With 6 quarks and 6 antiquarks this adds up to 12 different quarks. Together with the leptons this leads to 24 different particles that make up all the matter in the universe.

Despite being able to describe the existence and behaviour of quarks, no quarks were directly observed yet, but they were found to be in bound states of two or three quarks. These bound states are called *hadrons* and seem to only occur in two different ways: As a bound state of three quarks, called *baryon* or as a quark-antiquark bound state, called *meson*, where all of these are color-neutral. The most famous hadrons are the proton, which consists of one down- and two up-quarks (notation: uud) and the neutron, that is made of two down- and one up-quark (notation: udd). A meson, that often shows up is for example the so called *pion*, which is the combination of up- and down-(anti)quarks and which comes in three different charges. In table 2.5 the quark configurations of the most important hadrons are listed. Notice, that the Δ^+ has the same quark composition as the proton, but is a higher mass spin-excitation state of the proton. For each hadron, there exists a respective antiparticle which consist of the "reversed" quark composition. For example $|\bar{K}^+\rangle = \overline{|u\bar{s}\rangle} = |\bar{u}s\rangle = |K^-\rangle$.

The proton is the only known stable hadron, that can exist as a free particle without decaying. In

Type	Name	Symbol	Quark Composition
Baryons	Proton	$\|p\rangle$	$\|uud\rangle$
	Neutron	$\|n\rangle$	$\|udd\rangle$
	positive Delta	$\|\Delta^+\rangle$	$\|uud\rangle$
Mesons	charged Pion	$\|\pi^+\rangle$	$\|u\bar{d}\rangle$
	neutral Pion	$\|\pi^0\rangle$	$1/\sqrt{2}\left(\|u\bar{u}\rangle - \|d\bar{d}\rangle\right)$
	charged Kaon	$\|K^+\rangle$	$\|u\bar{s}\rangle$
	neutral Kaon	$\|K^0\rangle$	$\|d\bar{s}\rangle$

Table 2.5: A selection of hadrons (Povh et al., 2014)

a certain bound state, for example in an atomic nucleus, neutrons are also stable, but free neutrons eventually decay into the lighter protons with a mean lifetime of around 15 minutes (Mann, 2010).

Gauge Bosons

As said before, besides the fermions, the building blocks of matter, there exists another particle type, the so called bosons. These particles are the mediators of the fundamental forces as described by the Standard Model. The concept of interactions happening by the exchange of particles, which are the quanta of the field mediating the corresponding force or interaction, is the basis of the field-theoretical description of the elementary particle physics. This is a prerequisite of being able to describe the interactions of particles in terms of more or less easy processes using the Feynman-rules, without having to solve the respective quantum mechanical field-equations. One of these rules, which indicates if an interaction is allowed or not, is that at every coupling process the quantum numbers as listed in tables 2.2 and 2.4 are conserved. A coupling process is a process, where a gauge boson couples to a fermion or another boson to mediate the respective force. In the image of Feynman diagrams this is called a *vertex* (Berger, 2014).

In table 2.1 the mediator particles to the fundamental forces were already given: The electromagnetic force is mediated by the *photon*, the strong force is carried by *gluons* and the weak force by the three gauge bosons called W^+, W^- and Z^0. Photons are massless and don't have a charge of any kind. Due to photons not having mass, the electromagnetic force has basically an infinite range ($\propto 1/r^2$, like gravity). As mediators of the strong force, gluons are coupling to the color charges of quarks. They carry both a color and an anticolor and it shows that there are 8 different states in which they appear (Povh et al., 2014). How these states are defined is a matter of convention, for example they could be:

$$R\bar{G}\,,\;\; R\bar{B}\,,\;\; G\bar{B}\,,\;\; G\bar{R}\,,\;\; B\bar{R}\,,\;\; B\bar{G}\,,\;\; \sqrt{1/2}\left(R\bar{R} - G\bar{G}\right)\,,\;\; \sqrt{1/6}\left(R\bar{R} + G\bar{G} - 2B\bar{B}\right) \tag{2.1}$$

For mediating the strong interaction, gluons are coupling to color charges analogously to photons coupling with electrical charge to mediate the electromagnetic force. Since gluons themselves are carrying color charges, they are interacting with each other as well, which is a major difference to electromagnetism. Now even though gluons are thought to not have any mass, the strong force is limited to a very small range of around 1 fm, due to their self-interacting behaviour. If gluons exceed this range, the energy of the respective color field is high enough, so that real quark-antiquark-pairs

are produced from the gluons and they are not mediators of the strong force anymore (Povh et al., 2014).

The weak interaction gets mediated by the exchange of 3 gauge bosons (W^+, W^- and Z^0), with each having a different electrical charge as indicated by the upper index. In contrast to photons and gluons, those bosons are not massless, but have very high masses in the range of $\sim 100\,\mathrm{GeV/c^2}$ (Berger, 2014). Due to their high mass, those particles only exist for a very short time, even compared to other processes on the elementary scale, which is the reason for the small range of the weak interaction of around $10^{-3}\,\mathrm{fm}$ (Povh et al., 2014). The precise masses have been measured to be (Athar and Singh, 2020):

$$M_W = 80.379 \pm 0.012\,\mathrm{GeV} \tag{2.2}$$

$$M_Z = 91.1876 \pm 0.0012\,\mathrm{GeV} \tag{2.3}$$

Those masses are a consequence of another type of boson and its associated field, the so called Higgs boson. The Higgs model was developed in 1964 and postulated the existence of a scalar field, that gives these bosons and other particles their masses. In the theory of electroweak interaction there are four Higgs-fields, from which three of the respective quanta, the Higgs bosons, get absorbed by the three gauge bosons of the weak interaction. The model predicts the exact masses of the W^+, W^- and Z^0 bosons, a massless photon and a remaining free Higgs-boson, which was discovered at CERN in 2012 (Povh et al., 2014). Togehter with the 24 fermions, 8 gluons, 3 weak gauge bosons and the photon, this gives us the entirety of the 37 known elementary particles.

2.1.2 Introduction to Neutrino Physics

Now that the basics of the Standard Model are known, a more in depth overview about the characteristics of neutrinos in general and their way of interacting through the weak force will be given.

Neutrinos: A Closer Look

First of all, we are going to look into the characteristics of neutrinos in more detail. The existence of a half spin particle, which interacts with the weak force and has a neutral electrical charge, was first proposed by Pauli in 1930 as a result of discrepancies in the energy conservation of a common decay of atomic nuclei. Today we believe the neutrinos to be the most abundant particles in the universe besides photons and it is estimated, that there is a number density of around 330 neutrinos per $\mathrm{cm^3}$ throughout the universe (Athar and Singh, 2020).

Neutrinos are the only electrically neutral fermions and like all fermions they are color neutral, which is the reason, why neutrinos only interact with the weak force. Nevertheless, due to the weak force's universal character, neutrinos are interacting with all other elementary particles. As already mentioned in the previous section, there are three known neutrino families described in the Standard Model: The electron-neutrino ν_e, the muon-neutrino ν_μ and the tau-neutrino ν_τ. Measurements of the decay width of the Z^0-resonance during e^+e^--collisions made it possible, to determine the number of neutrino families, with the most current value being $N_\nu = 2.984 \pm 0.008$, which is at good agreement of the three families described in the Standard Model (Oberauer and Oberauer, 2019). In figure 2.1 you can see the results of such measurements from the ALEPH collaboration from 1992.

So the experiments are supporting the existence of three neutrino families which are coupling to the three gauge bosons of the weak force, which agrees with the specification of the Standard Model.

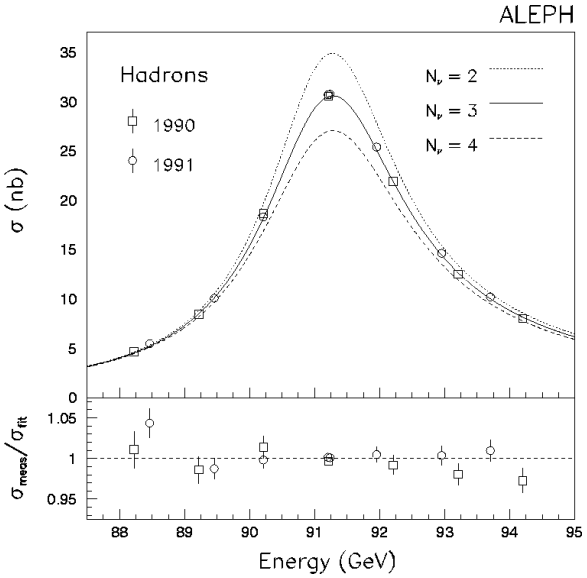

Figure 2.1: Ratio of measured over expected cross section for 3 neutrino families (ALEPH, 1992)

The theoretical description of such particles will be motivated in the following. Like all fermions, neutrinos are particles that satisfy the Dirac equation and therefore the wavefunction describing a free neutrino has to be a Lorentz-invariant solution to the following equation, with the Dirac matrices γ_μ, the scalar rest mass m, the index $\mu = 1, ..., 4$ and the four-vector $x = (x_1.x_2, x_3, x_4) = (t, \vec{x})$.

$$\left(i\gamma_\mu \frac{\partial}{\partial x_\mu} - m\right)\psi = 0 \tag{2.4}$$

In the Standard Model the rest mass of neutrinos is predicted to be $m = 0$, but experiments show that neutrinos have in fact a non zero rest mass, even if it is very small.

The solutions to the Dirac equation gives us the following wavefunction ψ:

$$\psi(x) \propto \begin{pmatrix} \hat{u} \\ (\nu\sigma)\hat{u} \end{pmatrix} e^{-ipx} + \begin{pmatrix} (\nu\sigma)\hat{v} \\ \hat{v} \end{pmatrix} e^{+ipx} \tag{2.5}$$

Here, $p = (E, \vec{p})$ is the four-momentum-vector, $E = \sqrt{p^2 + m^2}$ is the particle's energy and $\nu = \vec{p}/E + m$. The two parts of this equation are the particle states with positive and negative energy. The first term is interpreted as the particle state and the second one as the corresponding antiparticle. $\hat{u}$ and $\hat{v}$ are describing the spin states.

Equation 2.5 describes how free neutrinos are moving through space and time with a fixed rest mass. The way the particle propagates is characterized by the momentum vector $\vec{p}$ and mass m. Because the mass does not change, this wavefunctions are called *mass eigenstates* (Oberauer and Oberauer, 2019). This will be important in the section about neutrino oscillations, where we will see that these mass eigenstates are not equal to the flavor eigenstates and that the flavor states can change while the particle is propagating through space. Quarks have a similar property, with the flavor eigenstates being different to the mass eigenstates and both being connected in a certain way.

Electroweak Theory

As already mentioned in subchapter 2.1.1, electromagnetism and the weak force can be seen as two parts of the same unified theory, which is called electroweak theory. This theory was developed in a series of seperate works, that were done by Sheldon Glashow, Abdus Salam and Steven Weinberg in the 1960's, which was awarded with the Nobel Prize in 1979. It is therefore also called Glashow-Weinberg-Salam (GWS) model. The theory unified the electromagnetic and weak interactions in a common formalism, which - among other things - predicted the so called *neutral current* (NC) for the first time. The theory also predicted, that the mediators of the weak interaction are bosons with very high masses (NobelPrize.org, 2022).

The theoretical description behind the electroweak theory has its origin in the principle of local gauge invariance of fundamental interactions. The masses of the corresponding gauge bosons are generated by applying the Higgs-mechanism and introducing the corresponding scalar field (Athar and Singh, 2020). Covering the mathematical ideas behind this approach would be over the scope of this work, which is why we will simply have a look at the final implications of said theory.

The idea is to introduce a new quantum number, the so called weak isospin. With the conservation laws that are followed during weak interactions, this leads to the existence of a boson triplet W^-, W^+ and W^0, with weak force g and the exsitence of a boson singulett called B^0, which has weak force g'. Now the photon and the Z^0-boson can be seen as orthogonally orientated linear combinations of B^0 and W^0 which both interact with fermions without changing their weak isospin and therefore their type. The mixing of those two states can mathematically be described as a rotation with the so called *weak mixing angle* (or also *Weinberg-angle*) θ_W (Povh et al., 2014):

$$|\gamma\rangle = \cos\theta_W \, |B^0\rangle + \sin\theta_W \, |W^0\rangle \tag{2.6}$$

$$|Z^0\rangle = -\sin\theta_W \, |B^0\rangle + \cos\theta_W \, |W^0\rangle \tag{2.7}$$

The weak coupling forces g and g' and the weak mixing angle θ_W are connected as follows:

$$\tan\theta_W = \frac{g'}{g} \ , \quad \sin\theta_W = \frac{g'}{\sqrt{g^2 + g'^2}} \tag{2.8}$$

And for the electrical charge e one can find:

$$e = g \cdot \sin\theta_W \tag{2.9}$$

The weak mixing angle can be determined using different approaches and it is mostly given as $\sin^2\theta_W$ instead of θ_W directly. The current best value is $\sin^2\theta_W = 0.22290 \pm 0.00030$ (NIST/CODATA, 2018). Due to the fact that the weak coupling constant which characterizes the strength of the weak interaction is proportional to the square of the weak charge g and the electromagnetic coupling constant to the square of the electrical charge e, this shows us that the weak coupling constant is more than 4 times stronger than the electromagnetic one. That the weak interaction nevertheless has a lower effective strength than the electromagnetic force at low energies has to do with the high mass of the gauge bosons, as already addressed in the previous section (Povh et al., 2014).

Charged and Neutral Current

One can separate the weak interactions into two types: The *charged current (CC)*, which refers to an interaction over a W^+ or W^- boson and the *neutral current (NC)*, that describes interactions that are mediated by the Z^0.

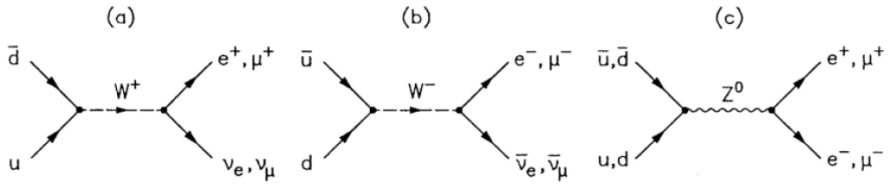

Figure 2.2: Lowest-order Feynman diagrams for the production of W^+, W^- and Z^0 bosons in proton-antiproton collisions and their respective leptonic decays (Zuber, 2020)

In the case of leptons, the CC-interactions take place within a particular generation, meaning for example the process $e^- \longrightarrow \nu_e + W^-$ is possible, but $e^- \longrightarrow \nu_\mu + W^-$ is not. For quarks, also couplings between different generations is possible, where for example both $d \longrightarrow u + W^-$ and $s \longrightarrow u + W^-$ are allowed interactions. However, the probability of couplings between quarks of different generations is significantly lower, especially when quarks of the third generation are involved. NC-interactions on the other hand do not change the flavor of a lepton or a quark, but can only change the energy of the respective particle. A real Z^0-boson, for example created in e^+e^--collisions, can decay into a lepton-antilepton or quark-antiquark pair. If no neutrinos are involved, all reactions can either take place via photon- or Z^0-exchange and it is not possible to determine the responsible mechanism for a single interaction (Griffiths, 2008). In figure 2.2, the lowest-order Feynman diagrams for the production of W^+, W^- and Z^0 bosons in proton-antiproton collisions, as well as their leptonic decays are shown, in order to highlight the different coupling properties.

2.1.3 Neutrino-Nucleus Interactions

When talking about neutrino interactions with matter, one can often find the Lagrangian of the electroweak interaction being given, which describes the kinematics and dynamics of the respective quantum system. Although this allows to qualitatively discuss the possible types of interactions (Oberauer and Oberauer, 2019), this is not very useful in practice. The theoretical description is an ideal one and needs to be corrected by a number of effects, such as unclear initial-state conditions, nuclear corrections or final-state interactions. When analysing the influences of such corrections and the validity of certain assumptions and simplifications, it shows that one can find very different descriptions of the scattering process when looking at different energy ranges (Formaggio and Zeller, 2012). We will therefore have a look at four different energy regimes and for each one the dominating interaction processes will be presented. The energy regimes are:

- Thresholdless processes: $E_\nu \approx 0 - 1\,\mathrm{MeV}$
- Low-energy nuclear processes: $E_\nu \approx 1 - 100\,\mathrm{MeV}$
- Intermediate-energy processes: $E_\nu \approx 0.1 - 20\,\mathrm{GeV}$
- High-energy processes: $E_\nu \approx 20 - 500\,\mathrm{GeV}$
- Ultra-high-energy processes: $E_\nu \approx 0.5\,\mathrm{TeV} - 1\,\mathrm{EeV}$

In the following, the dominant scattering processes in the respective energy ranges will be presented and their role in neutrino detection experiments outlined. The focus is set on the GeV range, so

intermediate- and high-energy processes, due to their importance in the study of neutrino oscillations.

Thresholdless processes: $E_\nu \approx 0 - 1\,\mathrm{MeV}$

This energy range covers the situations where the neutrino has essentially zero momentum. The interaction processes in this energy regime are *coherent scattering* and *neutino capture* on radioactive nuclei. Coherent scattering denotes the "neutral-current exchange where a neutrino interacts coherently with the nucleus" (Formaggio and Zeller, 2012). This means, the neutrino is interacting with the nucleus in a whole, without feeling individual effects of its constituents:

$$\nu + {}^{\mathrm{Z}}_{\mathrm{N}}\mathrm{A} \longrightarrow \nu + {}^{\mathrm{Z}}_{\mathrm{N}}\mathrm{A}^{*} \tag{2.10}$$

The measurement of this process was first achieved in 2017 (Zuber, 2020). Neutrino capture on radioactive nuclei (also: stimulated beta decay) is quite similar to the ordinary beta decay, but instead of having an anti-electron-neutrino $\bar{\nu}_e$ leaving the interaction, an electron-neutrino ν_e is interacting with the target nucleus (Formaggio and Zeller, 2012):

$$\nu_e + {}^{\mathrm{Z}}_{\mathrm{N}}\mathrm{A} \longrightarrow e^{-} + {}^{\mathrm{Z+1}}_{\mathrm{N-1}}\mathrm{A} \tag{2.11}$$

The problem with this reaction is, that it produces the same detectable components (e^- and ${}^{\mathrm{Z+1}}_{\mathrm{N-1}}\mathrm{A}$) as the regular beta decay. This process has not yet been observed.

Low-energy nuclear processes: $E_\nu \approx 1 - 100\,\mathrm{MeV}$

With higher energies, the lengthscales of the interactions become smaller and smaller, which results in the neutrino reacting with individual nucleons (protons and neutrons) rather than feeling the nucleus as a whole. This offers experimentalists the chance to probe a target nucleus on a fine level, which has already been extensively studied. The main reaction of concern is antineutrino-proton scattering, also known as inverse beta decay. This process is one of the simplest nuclear reactions and can be studied using neutrinos produced in nuclear fission reactors, which is why it is one of the earliest reaction to be analysed (Formaggio and Zeller, 2012).

$$\bar{\nu}_e + p \longrightarrow e^{+} + n \tag{2.12}$$

The process can be observed at neutrino energies above the threshold energy of $E_\nu^{thresh} = 1.806\,\mathrm{MeV}$, due to the mass difference between the proton and the neutron-positron-pair.

Intermediate-energy processes: $E_\nu \approx 0.1 - 20\,\mathrm{GeV}$

With further increasing energy, the description of neutrino-nucleus interactions becomes more variant and difficult, since a number of scattering processes become relevant at these energies. This is also the energy range, that is most important for the study of neutrino oscillations and will therefore be looked at in a bit more detail. In general, the interaction processes fall in three different categories: *Elastic and quasielastic scattering*, *resonance production* and *deep inelastic scattering*.

Elastic and quasielastic scattering describes the interaction with a nucleon, where the neutrino scatters off elastically and removes one or more nucleons from the target nucleus (Formaggio and Zeller, 2012). In the case of a CC interaction, the incoming neutrino converts to the charged lepton

of the respective lepton generation through the exchange of a W^- or W^+ boson. The following processes occur (Zuber, 2020):

$$\nu_l + p \longrightarrow l^- + n \tag{2.13}$$

$$\bar{\nu}_l + n \longrightarrow l^+ + p \tag{2.14}$$

CC quasieleastic scattering plays a big role for neutrino experiments, since the outgoing nucleon determines if there was a neutrino or an antineutrino and the relatively simple kinematics allow an easy reconstruction of the neutrino energy (Ereditato, 2018). For NC interactions, the neutrino only transfers energy to the nucleon via Z^0 exchange.

At high enough energies, the neutrinos can excite the target nucleon into a resonant baryon state, which is referred to as resonance production. For CC interactions, the reaction produces the corresponding charged lepton and the resonance, whereas for NC interactions this changes the energy of the neutrino and produces a resonance:

$$\nu_l + N \longrightarrow l^- + N^* \quad \text{(CC)} \tag{2.15}$$

$$\nu + N \longrightarrow \nu + N^* \quad \text{(NC)} \tag{2.16}$$

The baryon resonance (N^*) quickly decays over the strong interaction, which produces a nucleon (N) and a correspondingly charged meson, mostly a pion (π), which is the lightest of all mesons and has a certain combination of quarks, dependent on its sate. See table 2.5 for an overview.

$$N^* \longrightarrow N + \pi \tag{2.17}$$

The final state nucleon can differ from the initial one and there are a number reaction channels with different pion-lepton-nucleon combinations. These interactions have become very important for the analysis of neutrino oscillations and the modelling of nuclear effects acting upon the pion production and its movement out of the nucleus towards the detector becomes more and more important (Formaggio and Zeller, 2012). As already mentioned in the introduction, this is also the main point behind implementing the GiBUU model into KM3NeT and the subject will therefore be discussed in the chapter about the simulation of neutrino-nucleus interactions.

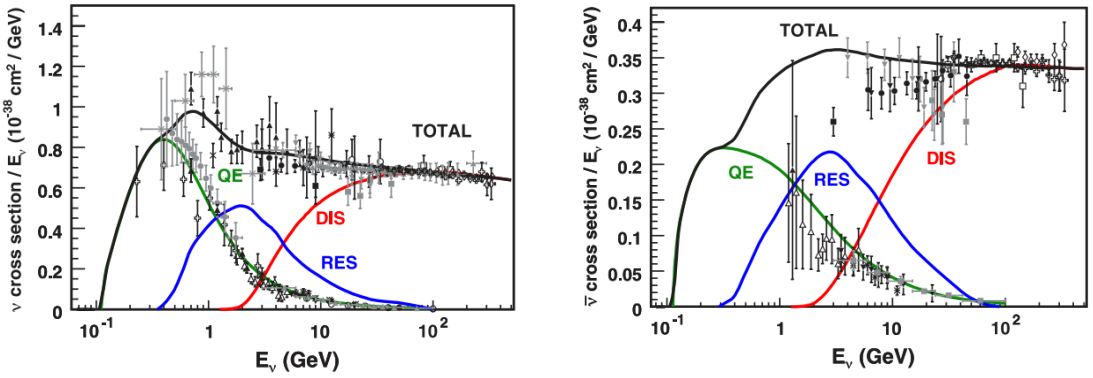

Figure 2.3: Total neutrino *(left)* and antineutrino *(right)* per nucleon cross sections for CC interaction on an isoscalar target divided by neutrino energy (Formaggio and Zeller, 2012)

With enough energy, the neutrino can interact with nuclei in such a way, that the scattering occurs with a quark inside the nucleons, which is known as deep inelastic scattering. The intermediate

energy range is a transition zone between elastic and deep inelastic scattering processes, where quasi-elastic, resonant and deep inelastic scattering all contribute to the interaction processes at a given energy. In figure 2.3 you can see the cross sections per nucleon divided by neutrino energy over the neutrino energy for neutrino- and antineutrino-nucleus interactions. The measurement data is combined from a number of works and compared to a prediction for each of the participating interaction processes, provided by the NUANCE generator (Formaggio and Zeller, 2012).

One can see, that in both cases the cross section approaches a linear dependency on the energy in the higher energy range, as it is expected when point-like sources dominate the interaction, as it is the case with deep inelastic scattering. Also, the figure outlines the importance of the energy band between 1 and 100 GeV, since there are most of the measurement points, which indicates the challenges when looking at very low energies. The same comparison can be made between neutrino and antineutro, where there are a lot more measurements made with neutrinos than for antineutrinos.

High-energy processes: $E_\nu \approx 20 - 500\,\mathrm{GeV}$

In this energy range, the previously mentioned process of deep inelastic scattering becomes more and more dominant, as you can also see from figure 2.3. The scattering happens both via CC and NC interaction, through W^+/W^- or Z^0 exchange, with both cases resulting in a lepton and a hadronic system. A single quark interacts with the neutrino and is released from its baryonic state as a nucleon (N). The quarks quickly recombine and can be observed as a hadronic shower (X) (Formaggio and Zeller, 2012).

$$\nu_l + N \longrightarrow l^- + X \quad \text{(CC)} \tag{2.18}$$

$$\bar{\nu}_l + N \longrightarrow l^+ + X \quad \text{(CC)} \tag{2.19}$$

$$\nu_l + N \longrightarrow \nu_l + X \quad \text{(NC)} \tag{2.20}$$

$$\bar{\nu}_l + N \longrightarrow \bar{\nu}_l + X \quad \text{(NC)} \tag{2.21}$$

This scattering event provides a good possibility to test the standard model and examine the deeper structure of nucleons, due to which it is a well studied process. For example have experiments with deep inelastic scattering of muons with nucleon targets lead to the experimental discovery, that nucleons are made up of point-like constituents that have spin 1/2: The quarks.

Ultra-high-energy processes: $E_\nu \approx 0.5\,\mathrm{TeV} - 1\,\mathrm{EeV}$

When reaching ultra-high energies, the linear relation between cross-section and neutrino energy is no longer present. The linearity initially comes from the mass of the weak gauge bosons dominating the interaction, which is no longer the case at ultra-high energies (Formaggio and Zeller, 2012).

2.1.4 Neutrino Oscillation and the Neutrino Mass Hierarchy

In the following, the mechanism behind neutrino oscillation will be presented. Furthermore, a short look on atmospheric neutrinos will be given and their role in the measurement of the neutrino mass hierarchy will be outlined.

Neutrino Oscillation

In chapter 2.1.1 the leptons were classified in three generations, where each generation contains one electrically charged and one neutral lepton. Those generations can be written in the form of family-dupletts:

$$\begin{pmatrix} \nu_e \\ e^- \end{pmatrix} \quad \begin{pmatrix} \nu_\mu \\ \mu^- \end{pmatrix} \quad \begin{pmatrix} \nu_\tau \\ \tau^- \end{pmatrix} \tag{2.22}$$

These neutrino flavor states $|\nu_e\rangle$, $|\nu_\mu\rangle$ and $|\nu_\tau\rangle$ are the eigenstates of the weak interaction. The weak interaction is coupling to the respective states in the way it is described in chapter 2.1.2. Neutrinos are generated in CC weak interactions and are always created in the form of a certain flavor eigenstate (Oberauer and Oberauer, 2019).

In chapter 2.1.2 the mass eigenstates were introduced, which are the solutions of the respective relativistic Dirac-equation. Those states have a defined mass and the solutions describe the propagation of free neutrinos and antineutrinos in space and time with their mass remaining unchanged during this evolution. There are also three of these mass eigenstates, called $|\nu_1\rangle$, $|\nu_2\rangle$ and $|\nu_3\rangle$ with mass eigenvalues m_1, m_2 and m_3. The flavor eigenstates $|\nu_\alpha\rangle$ are not the same as the mass eigenstates $|\nu_i\rangle$, but can be seen as a linear superposition of them (Oberauer and Oberauer, 2019):

$$\nu_\alpha = \sum_{i=1}^{3} U_{\alpha i} \nu_i \tag{2.23}$$

This has the consequence, that the flavor eigenstates don't have a defined mass, but only probabilities to have a certain mass at a given time. The connection between the flavor eigenstates and the mass eigenstates can be written in the form of a matrix $U_{\alpha i}$ that is called the leptonic mixing matrix:

$$\begin{pmatrix} \nu_e \\ \nu_\mu \\ \nu_\tau \end{pmatrix} = \begin{pmatrix} U_{e1} & U_{e2} & U_{e3} \\ U_{\mu 1} & U_{\mu 2} & U_{\mu 3} \\ U_{\tau 1} & U_{\tau 2} & U_{\tau 3} \end{pmatrix} \times \begin{pmatrix} \nu_1 \\ \nu_2 \\ \nu_3 \end{pmatrix} \tag{2.24}$$

The matrix $U_{\alpha i}$ is often also called Pontecorvo-Maki-Nakagawa-Sakata- or PMNS-matrix U_{PMNS} after Bruno Pontecorvo, who first predicted the phenomenon of neutrino oscillation in 1959 and Ziro Maki, Masami Nakagawa and Shoichi Sakata, who introduced this matrix as an explanation in 1962 (Povh et al., 2014).

The matrix has three real degrees of freedom θ_{12}, θ_{13} and θ_{23}, that can be interpreted as angles of rotation and are often called mixing-angles. In addition to that, there is one imaginary phase δ, which is connected to the CP-violation of the weak interaction. The matrix can be parameterized as follows, with $s_{ij} = \sin\theta_{ij}$ and $c_{ij} = \cos\theta_{ij}$ (Oberauer and Oberauer, 2019).

$$\begin{pmatrix} 1 & 0 & 0 \\ 0 & c_{23} & s_{23} \\ 0 & -s_{23} & c_{23} \end{pmatrix} \begin{pmatrix} c_{13} & 0 & s_{13}e^{i\delta} \\ 0 & 1 & 0 \\ -s_{13}e^{i\delta} & 0 & c_{13} \end{pmatrix} \begin{pmatrix} c_{12} & s_{12} & 0 \\ -s_{12} & c_{12} & 0 \\ 0 & 0 & 1 \end{pmatrix} \tag{2.25}$$

By multiplying out this matrices, we can find the individual mixing elements of the PMNS-matrix:

$$\begin{pmatrix} U_{e1} & U_{e2} & U_{e3} \\ U_{\mu 1} & U_{\mu 2} & U_{\mu 3} \\ U_{\tau 1} & U_{\tau 2} & U_{\tau 3} \end{pmatrix} = \begin{pmatrix} c_{12}c_{13} & s_{12}c_{13} & s_{13}e^{-i\delta} \\ -s_{12}c_{23} - c_{12}s_{23}s_{13}e^{i\delta} & c_{12}c_{23} - s_{12}s_{23}s_{13}e^{i\delta} & s_{23}c_{13} \\ s_{12}s_{23} - c_{12}c_{23}s_{13}e^{i\delta} & -c_{12}s_{23} - s_{12}c_{23}s_{13}e^{i\delta} & c_{23}c_{13} \end{pmatrix} \tag{2.26}$$

From this connection between flavor and mass eigenstates, one can see how the flavor eigenstates evolve over time, when a neutrino is propagating through space. The propagation is described by

the mass eigenstates, as shown in equation 2.5. For a neutrino (as opposed to an antineutrino) the solution of the dirac equation are plane waves in the following form:

$$\nu_i(t) = \nu_i(t=0) \cdot e^{-i(E_i t - p_i x)} \qquad (i = 1, 2, 3) \tag{2.27}$$

Now imagine a neutrino being created at $t = 0$ with a certain flavor eigenstate. If E_i and p_i are not equal for all i, then the values for the phases $\nu_i(t)$ will evolve differently. This is the case, if not all m_i are the same, meaning not all mass eigenstates have the same mass. Since different phases $\nu_i(t)$ at a given time change the composition of the superposition, this will lead to the probability of detecting a neutrino in a certain flavor eigenstate ν_α to change periodically during the propagation. This effect is called *neutrino oscillation* (Oberauer and Oberauer, 2019).

With the high relativistic approximation ($E_i \approx p + m_i^2/2p$), the wave function of a certain neutrino flavor ν_α that is created at time $t = 0$ at $x = 0$ and is now travelling through a vacuum is given as follows:

$$\psi(x,t) = e^{ipx} \sum_i U_{\alpha i} e^{-i\left(m_i^2 t/2p\right)} \nu_i \tag{2.28}$$

One can show, that the probability of detecting, for example an electron neutrino ν_e at a certain point x at time t again with flavor state ν_e is given by:

$$P_{e,e}(x,t) = 1 - P_{21} - P_{31} - P_{32} \tag{2.29}$$

$$P_{21} = 4\,|U_{e1}|^2 |U_{e2}|^2 \sin^2 \Delta_{21} \tag{2.30}$$

$$P_{31} = 4\,|U_{e1}|^2 |U_{e3}|^2 \sin^2 \Delta_{31} \tag{2.31}$$

$$P_{32} = 4\,|U_{e2}|^2 |U_{e3}|^2 \sin^2 \Delta_{32} \tag{2.32}$$

$$\Delta_{ji} = \frac{\Delta m_{ji}^2 x}{4p} \tag{2.33}$$

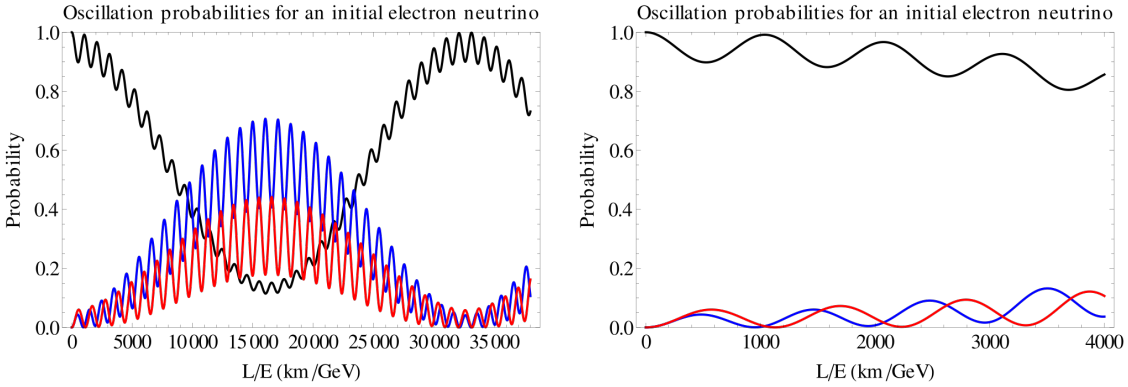

Figure 2.4: Oscillation probabilities for an initial electron neutrino in long range *(left)* and short range *(right)*. The colors represent the neutrino flavors: black: ν_e, blue: ν_μ and red: ν_τ (Wikipedia, 2011)

The whole process of neutrino oscillation as described by this formalism is only causing this oscillating change in the detection probability of a certain flavor, when neutrinos are not massless and do not all have the same mass $m_i = m$. Past experiments could clearly show this behaviour and it is therefore

seen as proven, that neutrinos are not massless, in contrary to how the Standard Model treats them and predicts them to be (Oberauer and Oberauer, 2019). In figure 2.4 the oscillation of an electron neutrino is shown in two length scales, the long range oscillation over the distance of 40000 km and the short range oscillation for a distance of 4000 km.

Atmospheric Neutrinos

The short range oscillation becomes important for the analysis of so called *atmospheric neutrinos*, that get created in the earth's atmosphere during the interaction with high energetic cosmic rays. These rays, which are dominantly high energetic protons or helium, are producing many secondary particles in strong interactions with the molecules of the upper atmosphere, which then decay further into neutrinos, which we call atmospheric neutrinos (Ereditato, 2018). In these strong interactions, mainly pions $\pi^{\pm}$ and kaons $K^{\pm}$ are produced. In the following, the dominant decay of these mesons are shown (Zuber, 2020):

$$\pi^- \longrightarrow \mu^- + \bar{\nu}_\mu \tag{2.34}$$

$$\pi^+ \longrightarrow \mu^+ + \nu_\mu \tag{2.35}$$

$$K^- \longrightarrow \mu^- + \bar{\nu}_\mu \tag{2.36}$$

$$K^+ \longrightarrow \mu^+ + \nu_\mu \tag{2.37}$$

The muons and antimuons created in these reactions will further decay and eventually produce more neutrinos:

$$\mu^- \longrightarrow e^- + \bar{\nu}_e + \nu_\mu \tag{2.38}$$

$$\mu^+ \longrightarrow e^+ + \nu_e + \bar{\nu}_\mu \tag{2.39}$$

In figure 2.5 the development of such a cosmic ray shower is visualized.

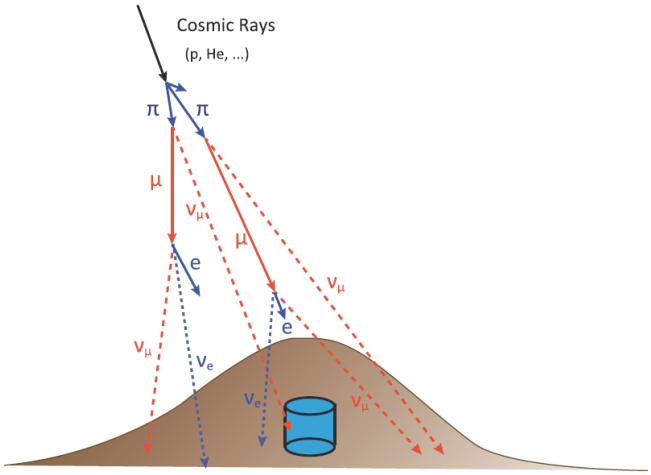

Figure 2.5: Illustration of a cosmic ray shower in the atmosphere (Ereditato, 2018)

When looking at the reaction chains one could expect twice as many muon neutrinos than electron neutrinos from cosmic ray showers arriving at the earth's surface, so $\nu_\mu : \nu_e \approx 2$. However, this is only reasonable for neutrino energies between around 0.1 GeV and 3 GeV, since with lower energies

the muon neutrino might decay before hitting the surface and with higher energies time dilatation starts to play a role and alters the expected value (Oberauer and Oberauer, 2019). In 1990, experiments at the Kamiokande detector showed, that the number of muon neutrinos was lower than expected, whereas the number of electron neutrinos was in agreement with the predictions. Further experiments, that compared the neutrino flux coming from above (directly from the atmosphere) and below (atmospheric neutrinos that have already traversed the earth) lead to strong indications, that the discrepancy could be explained by a possible neutrino oscillation and the flavor change $\nu_\mu \longrightarrow \nu_\tau$ (Ereditato, 2018). This discovery was awarded with the Nobel Prize in 1999.

Neutrino Mass Hierarchy

As you can see from equations 2.29 to 2.33, the probability of detecting a - in this case - electron neutrino in the same flavor state (which is also called *survivalprobability*) depends on the mass differences $\Delta m^2_{21} = m^2_2 - m^2_1$, $\Delta m^2_{31} = m^2_3 - m^2_1$ and $\Delta m^2_{32} = m^2_3 - m^2_2$. Note, that only two of them are independent, since $\Delta_{31} = \Delta_{32} + \Delta_{21}$ (Oberauer and Oberauer, 2019).

The analysis of neutrino oscillation experiments offers the possibility to determine the Δm^2_{ji} values, the mixing angles θ_{ij} and the CP-violation phase δ. With the current data, two different variations of the neutrino mass hierarchy (NMH) are possible, with the variations being called *normal hierarchy* for $\nu_1 < \nu_2 < \nu_3$ and *inverted hierarchy* for $\nu_3 < \nu_1 < \nu_2$. In figure 2.6 mass spectra of both variants are illustrated for the case of an initial electron neutrino (Ereditato, 2018). One way of measuring the NMH is to analyse atmospheric neutrinos that have travelled through the earth, which is also the approach used in KM3NeT. This will be discussed in more detail at the end of the next chapter.

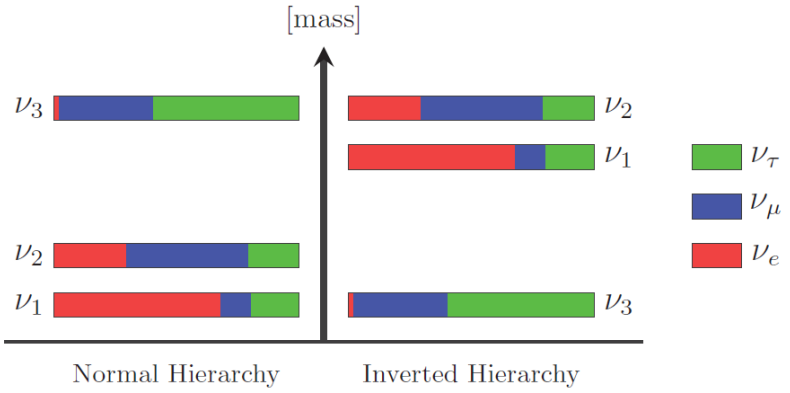

Figure 2.6: Neutrino mass hierarchy spectra for normal hierarchy *(left)* and inverted hierarchy *(right)*. The color bars represent the flavor content existent in each mass eigenstate for the evolution of an electron neutrino ν_e (Ereditato, 2018)

Determining the NMH is of great importance for the field of particle physics. On one hand, the NMH is the basis for being able to process data from neutrino experiments and a precise knowledge will lead to an optimized analysis of such experiments. This includes experiments regarding the CP-violation-phase δ, searches for the absolute neutrino masses and possible violations of the conservation of the lepton number in the so called neutrinoless double-beta decay, which could reveal more information about the true nature of neutrinos (Oberauer and Oberauer, 2019). On the other hand, this could

help to evaluate or even reject different models regarding the measurement of the neutrino masses. It is also an important parameter in different cosmological models and its identification plays a crucial part in next level neutrino experiments and the evaluation of cosmological data, what could possibly lead to the detection of new physics (Winter, 2015).

Current Knowledge?

2.1.5 Detection of Atmospheric Neutrinos

In the following section, the detection mechanism for the analysis of atmospheric neutrino oscillation will be outlined. First the process of Cherenkov-radiation will be presented and afterwards the general structure and analysis approach of a neutrino telescope will be elaborated, before having a look at the investigation of atmospheric neutrinos, as it is also done by KM3NeT/ORCA.

Cherenkov Effect

In order to understand the detection principle of neutrino telescopes like KM3NeT, one has to be familiar with the so called *Cherenkov effect*. The effect was first experimentally detected by Pavel Cherenkov in 1934 and in 1937 a theory describing this effect was developed by Igor Tamm and Il'ja Frank, for which those three were awarded the Nobel Prize in 1958. The effect describes the electromagnetic radiation (so called *Cherenkov radiation*) that is emitted, when a high energetic charged particle is travelling through a dielectric medium at a speed, that exceeds the phase velocity of light in that medium (Bashmakov, 2015). A famous example for this radiation, is the blue glow in the water surrounding the core of an atomic reactor.

If a pointlike charge is travelling through a medium, the atoms the particle is passing by get polarized by the electromagnetic field of the moving charge, what causes them to emit photons as they return to their ground state (Bashmakov, 2015).

Those photons can be described as spherical waves and the superposition of these waves overlays with phase shifts, originating from the particle's movement, that depend on the particle velocity v and the phase velocity of light $c_n = c/n$ in the medium, where n is the diffraction index of said medium. For $v < c_n$, the individual waves can't overlay with the same phase, what leads to destructive interference and therefore no emission of light. If the velocity of the particle exceeds the phase speed of light, there exists an angle ϑ_C with respect to the propagation direction of the particle, at which all waves interfere constructively, leading to the emission of Cherenkov radiation in a characteristic orientation. The Cherenkov radiation gets emitted in the form of a cone, which can also be motivated by Huygen's principle of the superposition of spherical waves coming from a source that moves faster than the phase velocity of these waves, as illustrated in figure 2.7 (Demtröder, 2017).

The opening angle of the light cone is connected with the particle's velocity and the phase speed of light in the respective medium in the following way:

$$\sin\vartheta_C = \frac{c_n}{v} = \frac{c}{n\dot{v}} = \frac{1}{\beta \cdot n} \quad \text{with} \quad \beta = \frac{v}{c} \tag{2.40}$$

This tells that only particles with $\beta \cdot n > 1$ will produce Cherenkov radiation (Demtröder, 2017). With the relativistic kinetic energy $E = mc^2(\gamma - 1)$, this condition leads to the minimal energy a

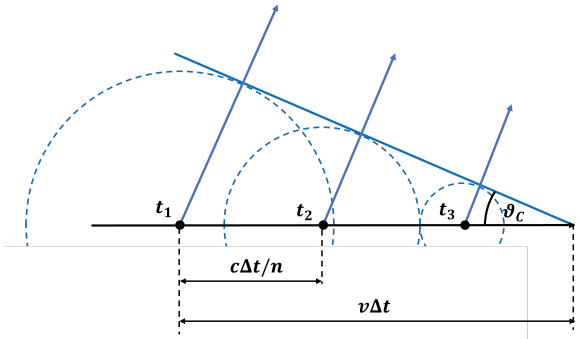

Figure 2.7: Illustration of the Cherenkov effect (based on Demtröder, 2017). Notice that the emission is of course symmetrical around the moving axis of the particle, forming a three dimensional cone

particle needs to have in order to emit Cherenkov radiation when travelling through a medium with refraction index n:

$$E_{min} = mc^2 \left(\frac{n}{\sqrt{n^2 - 1}} - 1 \right) \tag{2.41}$$

Due to this property, detectors which rely on Cherenkov radiation coming from particles can be used as threshold detectors, that only detect charged particles with the respective energy (Demtröder, 2017). From the connection between opening angle and velocity, it can be reconstructed from detecting the respective photons and determining the opening angle. Also, the distribution of measured photons allows to draw conclusions regarding the particle type. For example, in figure 2.8 the detection patterns (also called *Cherenkov rings*) of a muon and an electron interacting with water is illustrated (Suekane, 2015).

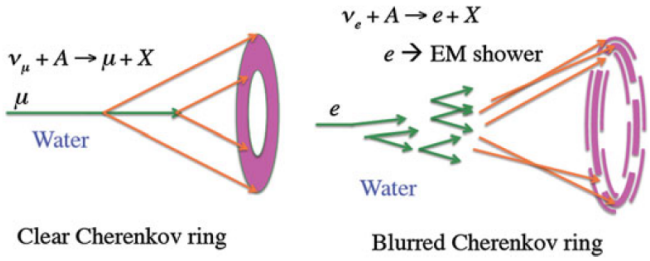

Figure 2.8: Illustration of the identification of a particle via their produced Cherenkov ring. Taken from (Suekane, 2015)

Underwater Cherenkov Neutrino Telescopes

Due to the small interaction cross-sections of neutrino interactions the detection is very difficult. In order to collect a significant data, the detection medium has to be very massive or stretch over a big amount of space. Also, the detectors should allow to reconstruct the paths of secondary particles generated in neutrino interactions. These requirements get satisfied by embedding a material, that

induces enough neutrino interactions, but on the other hand allows the transit of secondary particles without too much further interaction in order to be able to reconstruct the initial neutrino's momentum and direction, inside a three dimensional detector structure. There's a number of approaches to this task, with one of them being *underwater Cherenkov neutrino telescopes* (Ereditato, 2018).

In general, underwater Cherenkov neutrino telescopes use the interaction of neutrinos with water and are detecting the Cherenkov radiation coming from charged particles, that got created during the interaction between the neutrino and the nuclei in the water. During further interactions of these particles with their surrounding, different reaction chains produce showerlike events, with detectable photons as final particles. The detection of these photons in three-dimensional detector arrays enables the spatial reconstruction of a certain event (Spiering, 2020).

Simulation Chain for Neutrino Telescopes

In this section, the typical simulation chain for neutrino telescopes will be presented. The focus is set on underwater cherenkov telescopes, but due to the neutrino's characteristics and the inability to directly measure them in a detector, most neutrino experiments use a similar approach. The process will be explained using KM3NeT/ORCA as an example. It consists of the following major stages, which are passed through step by step (Hallmann, 2021):

1. **Generation:** The neutrino flux is modelled after the existent specification and the interactions of these neutrinos with the nuclei of the respective target material are simulated. The result of this stage are a number of interaction events, where for each initial neutrino the outgoing particles of the reaction are simulated.
2. **Propagation:** The propagation and further decay of these particles is simulated, resulting in a description of the photons produced in the interaction or decays of secondary particles. The further propagation of this light through the detector volume is modelled.
3. **Triggering:** An additional background light is simulated and the response of the detector (in this case photo-multiplier-tubes) are modelled. The software algorithms used in the telescope for triggering the detection of an event is applied to the modelled response, which leads to a data output in the same way it is expected by the real telescope when detecting real events. After this step, the simulated data gets handled in the same way as real data.
4. **Reconstruction:** A number of algorithms are applied, in order to reconstruct track or shower events from the respective photon data. In a way this is the reverse process of the three previous stages, since the only available data is the response of the detectors to the photons that emerged from a neutrino-nucleus interaction, with the goal to identify the energy, momentum and type of the incoming neutrino and the respective particles participating in the interaction.
5. **Event Identification:** In order to assure the correctness of the reconstruction process, a machine learning algorithm is applied to the final data, which allows to fine tune the reconstruction process with regard to the particles simulated in the generation stage. This allows for the classification of the reconstructed events.
6. **Analysis:** The output can then further be analysed and manipulated for the usage in sophisticated physics analysis.

Overall, this aims at measuring neutrinos that interact with the target material in a way that they call detectable particles, in this case photons. Comparing the measurement results to models

describing the evolution of atmospheric neutrinos during their journey through the earth (or the respective process a neutrino experiment is looking at) enables an in depth analysis of this process.

2.2 The KM3NeT Neutrino Telescope

In this chapter, the working principle and the goals of the KM3NeT Neutrino Telescope will be presented.

Overview and Goals

The KM3NeT (which stands for *cubic kilometer neutrino telescope*) collaboration was founded for planning and executing the construction and operation of a new neutrino research infrastructure in the Mediterranean Sea. It builds upon the experience made with the first generation of Cherenkov detectors in the Mediterranean Sea, namely *NESTOR*, *NEMO* and *ANTARES*. It is planned to install a number of building blocks on three off-shore sites: Near Toulon in France, Capo Passero in Italy and Pylos in Greece. Each building block serves as a "3-dimensional-array of photo sensors that can be used to detect the Cherenkov light produced by relativistic particles emerging from neutrino interactions" (Adriá n-Martínez et al., 2016). The project is a collaboration of many research institutes in Europe and around the world. In figure 2.9 the locations of the member institutes, as well as the planned detector installation sites are shown. The off-shore site in Greece will be subject of future phases of the project and currently the constructions are concentrated on the sites in France and Italy.

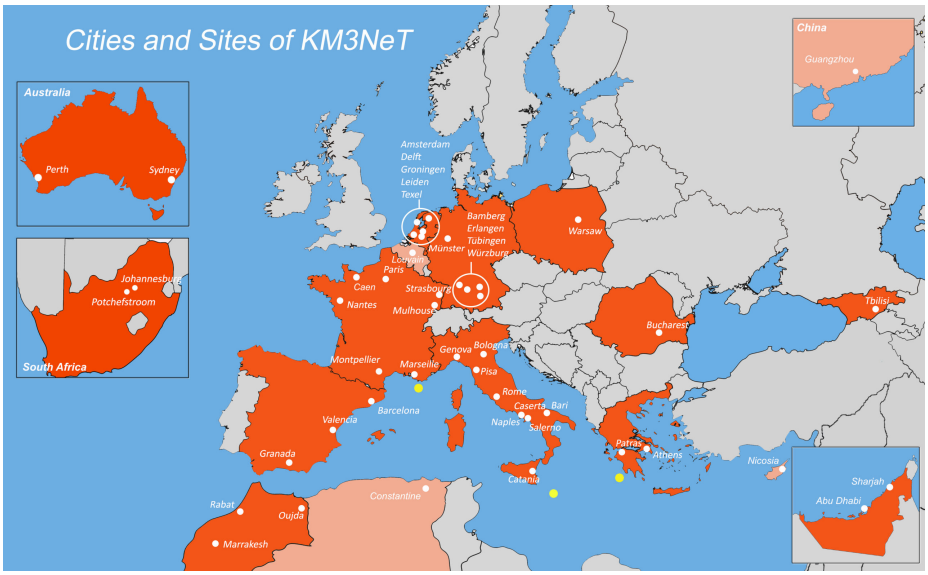

Figure 2.9: Cities and sites of KM3NeT. The off-shore sites where the detectors will be located are marked in yellow (KM3NeT-Collaboration, 2022a)

The main goals of KM3NeT are:

- The discovery and deeper analysis of high-energy neutrino sources

- The determination of the neutrino-mass-hierarchy

Two of the currently constructed building blocks will be configured to study high-energy neutrino sources and are collectively referred to as ARCA (Astroparticle Research with Cosmics in the Abyss). They are realized at the italian off-shore site near Capo Passo. The other building block is designed to study the oscillation of atmospheric neutrinos in order to further analyse the neutrino-mass-hierarchy. This one is called ORCA (Oscillation Research with Cosmics in the Abyss) and it will be located at the off-shore site near Toulon in France and will be part of the *Mediterranean Eurocentre for Underwater Sciences and Technologies*. ORCA is placed around 10 km west of the existing ANTARES detector, both of which can be seen in the map in figure 2.10. You can also see the planned geometry of the finished ORCA detector (Adriá n-Martínez et al., 2016).

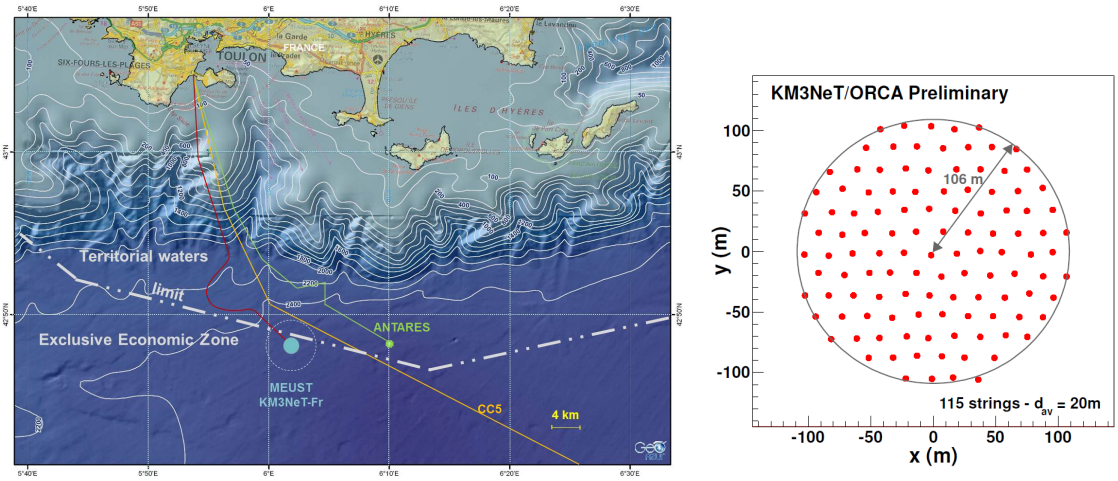

Figure 2.10: Map of the Mediterranean Sea south of Toulon with the location of the ORCA ("MEUST KM3NeT-Fr") and the ANTARES detector *(left)* and the top view of the planned ORCA detector. The geometry of the full detector will be a zylinder with $R = 106\,\mathrm{m}$ and $z = 102\,\mathrm{m}$. The instrumented volume is $V = 3.6 \times 10^6\,\mathrm{m}^3$ (Adriá n-Martínez et al., 2016)

Detector Components

Each building block consists of 115 evenly spaced strings, that are attached to the seafloor, with each string containing 18 digital optical modules (DOMs) that are distributed over the height of the string. The other side of the string contains a submerged buoy, which will hold the strings in a vertical orientation. Each DOM is made up of 31 photo-multiplier tubes (PMTs), that are spherically arranged, as well as their associated readout electronics and three sensors: One LED beacon to calibrate their position with respect to the other DOMs above them, one compass and tilt-meter to calibrate their general orientation and one acoustic piezo sensor for position calibration (Adriá n-Martínez et al., 2016). In figure 2.11 you can see a sketch of the arrangement of the DOMs on one string, as well as the picture of one DOM.

In general, the technology and the detection principle for ARCA and ORCA is the same. This is also one of the goals behind the detector design, that one can use a standardized equipment for different fields of study. The arrangement of the strings with respect to each other, as well as the placement

Figure 2.11: Sketch of a KM3NeT detection string *(left)* and a picture of a DOM *(right)* (Adriá n-Martínez et al., 2016)

of DOMs over one string depends on the science goals, for which the respective building block is designed. With ARCA being designed for the study of high-energetic particles (TeV- to PeV-range) a less dense spacing of the DOMs is chosen, whereas ORCA needs to be more sensitive to lower energetic neutrinos (low GeV-range) and will therefor be more densely packed. More specifically, the strings in ORCA are spaced 20 m apart from each other (in ARCA 90 m) and the DOMs are verticaly spaced with 9 m distance (in ARCA 36 m). The ORCA block will be deployed at a depth of 2450 m around 40 km off the coast from Toulon. ARCA will be localised 100 km offshore from Capo Passero at a depth of 3500 m (Adriá n-Martínez et al., 2016).

Data Acquisition

The signals detected by the PMTs are digitised right in the respective DOM. if the signal exceeds a specific threshold, before being sent to a facility on shore where the data gets further processed in real time. The data transfer happens via a network of electro-optical fibres, where each DOM has a unique wavelength, which allows the simultaneous transmission of many DOM signals at once (Adriá n-Martínez et al., 2016). On shore, the cables are connected to a power station from where the signal

gets sent to the respective facility via land cable. There, a PC farm is located, on which dedicated software is applying a first selection of hits, background reduction and event reconstruction. This data is then sent via 10 GB/s link to the KM3NeT data repository at the IN2P3 computing centre in Lyon (KM3NeT-Collaboration, 2022b).

2.3 Simulating Neutrino-Nucleus Interactions

As presented in subsection 2.1.5, an important step in the analysis chain of a neutrino experiment is to adequately simulate the interaction process of the neutrinos with the atomic nuclei of the target material. Due to the complexity and the high number of these events, the simulations have to be made based on certain assumptions or simplifications in order to allow for a reasonable computation time. Currently, KM3NeT is using an application, that is based on the GENIE neutrino monte carlo generator, in order to generate high statistics samples of detectable events, that originate from neutrino interactions. GENIE is using parameterised models for different interaction processes and initial neutrino energies (Aiello et al., 2020). However, studies were made by Schumann and Jung, 2021 to include another neutrino event generator into the KM3NeT analysis chain, which is called GiBUU. This generator includes simulating the propagation of secondary particles from initial neutrino interactions through the potential of the nucleus, using the *Boltzmann-Uehling-Uhlenbeck (BUU) equation*, accounting for final state interactions (Leitner, 2009). In the following, an overview about both event generators will be presented.

2.3.1 GENIE/gSeaGen

GENIE (which stands for *Generates Events for Neutrino Interaction Experiments*) is a neutrino event generator, which allows to simulate neutrino interactions for neutrinos of all flavors with energies from the MeV to the PeV energy range and it is also valid for a variety of target materials. However, it focuses on simulations in water and interactions of neutrinos in the few-GeV range (Andreopoulos et al., 2010).

As you could see from subchapter 2.1.3, the description of neutrino-nucleus interactions depends strongly on the neutrino's initial energy, which is why theoretical models describing such interaction processes are often limited to a small energy and particle type range and therefore only describes a small subset of all possible interactions. With the attempt to describe interactions of multiple particle types in all energy ranges, GIBBU combines a number of different models, including different nuclear physics descriptions, different cross-section models for various scattering types and energies and different approaches for modelling the production of hadronic showers. It allows to simulate neutrino flux coming from pointlike sources or from a distributed source region, which is the case for atmospheric neutrino studies (Andreopoulos et al., 2010).

Since the energy range for analysing neutrino oscillations is in the lower GeV range, where a number of different scattering processes have to be taken into account, the selection of the right model is of great importance in order to ensure the physical validity of every model for each neutrino energy and to avoid double counting of different models, that describe the same physical process behind it but are fine tuned for different energies (Andreopoulos et al., 2010).

This is a general problem for the most simulations of particle interactions, that are designed to apply to a broad energy and particle range and most sophisticated neutrino event generators used in neutrino experiments use this approach. A main difference in modelling neutrino-nucleus scattering

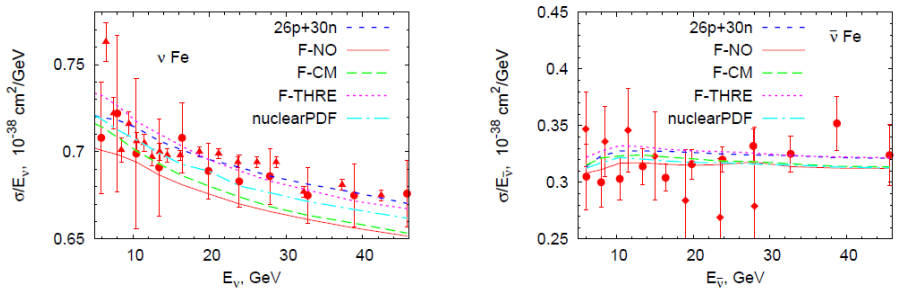

Figure 2.12: Total cross section per nucleon for reactions induced by neutrino *(left)* and antineutrino *(right)* interactions with an iron target. The *nuclearPDF* combines the three cross sections *F-NO*, *F-CM* and *F-THRE*. *26p+30n* shows the free cross section of iron composition (Lalakulich, 2011)

processes is the treating of the final state interactions, which has been a major field of study in the past years (Andreopoulos et al., 2010).

The GENIE code is implemented into the KM3NeT analysis chain, by wrapping it inside an application called gSeaGen, which allows to generate the neutrino flux with GENIE over a parametrized model of the expected neutrino flux coming from atomspheric neutrinos who have traversed earth in order to enable the study of oscillation data with the KM3NeT telescope (Aiello et al., 2020).

2.3.2 GiBUU/KM3BUU

The GiBUU (which stands for *Giessen Boltzmann-Uehling-Uhlenbeck*-model was developed at the Justus-Liebig-Univertiy in Giessen and initially build to describe heavy-ion collisions. The model has then been extended by the description of other high energy interactions including neutrino induced reactions for energies in the GeV range (Leitner, 2009).

The model uses a similar approach as GENIE regarding the simulation of the initial scattering event, calculating the interaction cross section as the sum of the scattering cross sections for quasielastic scattering, resonance production and deep-inelastic scattering as well as several background processes. In this first interaction step, a number of nuclear effects are taken into account as well. Such effects account for effects during particle-nucleon interactions, that originate from the nucleons being bound in a nucleus, like for example Pauli-blocking of the final-state nucleons or the effects coming from the nucleus' mean potential. The special part of this model however is the treatment of the particles propagation out of the nucleus, where further final-state interactions occur (Leitner, 2009). In figure 2.12 the calculated total cross section is shown together with data from MINOS and IHEP-JINR. The important part is the good agreement of the "nuclearPDF" with the data.

In the GiBUU model, these final-state interactions are treated in the framework of coupled-channel transport theory on the basis of the BUU-equation. This approach includes a number of coupled-channel effects, for example "elastic and inelastic scattering, charge-exchange scattering, resonance production and decays in the medium" and allows for the realistic microscopic description of the final-state interaction process in the presence of the nucleus' mean field (Leitner, 2009).

The BUU-equation, which is implemented for this description, "describes the space-time evolution of a many-particle system under the influence of mean-field potentials" (Leitner, 2009). The formalism

treats a system of particles, which is characterized by the one-particle distribution functions of the participating particles, so that the time evolution of this system can be described by a kinetic equation. Using the hydrodynamic formalism, that deals with the relaxation of a fluid from a perturbed state back into equilibrium, this allows for a very detailed description of multi-channel interaction systems in a mean field (Torres-Rincon, 2014). Due to the high complexity of this subject, outlining the actual mathematical concepts would go way beyond the scope of this paper. Since the structure of the equation is not very meaningful without deeper exploration of the underlying formalism and probably only causes confusion, it is not seen as useful here.

3 Data Analysis

With the theoretical basics behind the study of neutrino oscillations with the KM3NeT telescope covered, we can move on to the practical part of this work. The goal is to analyse the implementation of GiBUU into the KM3NeT analysis chain with the KM3BUU software package. A number of parameters will be analysed using high statistical data and the analysis will be contrasted with respective data from gSeaGen, which is already validated for the use in the simulation chain. This provides the opportunity to evaluate the performance of GiBUU in the context of the KM3NeT data framework and to see if there are significant differences between both generators and for the general comparison of data from different event generators.

3.1 Data Overview

In the following, a short overview about the data used in this work will be given. The neutrino flavors, neutrino energies, interaction types and target composition will be presented. Notice that besides bigger energy ranges being available for both generators, a cut was applied to all data sets, in order to reduce it to a range of 1 to 100 GeV, which is the overlapping energy range of both generators. During the analysis the data was further reduced to the range of 1 to 10 GeV for ensuring a direct comparability of the data sets.

For both cases the neutrino generation was set to model the detection volume of ORCA as it is specified in figure 2.10, with the interaction medium being seawater. The number of events generated is different for both generators, simply due to the respective settings when computing the simulations. However, all histograms are normalized and for both cases the same bins were applied. Together with the consistent energy range the data was restrained to and the respective treatment of the corresponding event weighting as described in section 4.1, this leads to a fully comparable data set enabling the evaluation of the GiBUU implementation with respect to the currently used gSeaGen code.

3.1.1 GENIE/gSeaGen

The gSeaGen data, that is used as a current reference and is used to compare it with the newly generated GiBUU data, had to be taken from past simulations that were done for the testing of the KM3NeT analysis chain. However, not all types of interactions for all neutrino flavors were available and in the right condition to work with, which limited the possible comparisons between both generators. The respective gSeaGen data that was used in this work is summarized in table 3.1. The column "Notation" specifies how the data is marked on the plots in order to allow a quick knowledge on which data you are looking at in each plot.

The target material was chosen by the gSeaGen default setting. In table 3.2 an overview about the target composition is given, which is supposed to model the mixture of sea water at the level of ORCA.

The gSeaGen data for muon CC runs was available in two different data sets for each interaction type, which were divided into the energy ranges 1 to 50 GeV and 50 to 500 GeV. The rest of the gSeaGen data was present as a single data set for each process over the energy range of 1 to 500

Neutrino Flavor	Interaction Type	Energy Range	Notation
ν_μ	CC	1-500 GeV	μ CC
$\bar{\nu}_\mu$	CC	1-500 GeV	anti μ CC
ν_μ	NC	1-500 GeV	μ NC
$\bar{\nu}_\mu$	NC	1-500 GeV	anti μ NC
ν_e	CC	1-500 GeV	e CC
$\bar{\nu}_e$	CC	1-500 GeV	anti e CC

Table 3.1: Overview of the gSeaGen data used in this work

Element	Percentage	Element	Percentage
^{16}O	85.84 %	^{32}S	0.091 %
^{1}H	10.82 %	^{40}Ca	0.04 %
^{35}Cl	1.94 %	^{39}K	0.04 %
^{23}Na	1.08 %	^{80}Br	0.0067 %
^{24}Mg	0.1292 %	^{12}C	0.0028 %

Table 3.2: Composition of the seawater target medium defined in gSeaGen (Aiello et al., 2020)

GeV. Unfortunately the gSeaGen NC interaction runs could not be analysed due to problems with the available files. Nevertheless the comparison of the other runs will allow a basic classification of GiBUU and KM3BUU with regard to their role as event generator in the Km3NeT simulation chain.

3.1.2 GiBUU/KM3BUU

For the GiBUU data, new runs were created for the use in this work. The generated runs are spread over an energy range from 0.5 GeV to 100 GeV and include both CC and NC reactions of all neutrino flavors. Each run was made for two different target materials, namely $^{16}_{8}$O and $^{1}_{1}$H, which are the main constitutes of water.

From table 3.2 you can see that the target mixture in gSeaGen is made up of more than 96 % of $^{16}_{8}$O and $^{1}_{1}$H, which is why the direct comparison of both data sets is still leading to valid qualitative statements regarding the implementation of GiBUU. However, it has to be kept in mind, that different processes that are not being looked at in the GiBUU cases are included in the gSeaGen data. The aim for the future is of course to simulate the target material in the GiBUU runs analogously to the gSeaGen runs in order to adequately model the interactions expected to be happening in the seawater. In table 3.3 an averview about the GiBUU data is given. The "Notation" term is again an indication for the respective interaction processes that can be found on the plot, in the same way as it is done for the gSeaGen data. Notice that the data for $^{16}_{8}$O and $^{1}_{1}$H is combined to form a comparable interaction situation, where the target material resembles water.

The GiBUU data was divided into two data sets for each process with one containing runs with energies from 0.5 to 10 GeV and the other one from 10 to 100 GeV. The data was present in two formats, one being the output provided by GiBUU and one containing files that are already converted into the KM3NeT data format with KM3BUU.

Neutrino Flavor	Interaction Type	Energy Range	Target material	Notation
ν_e	CC	0.5-100 GeV	^{16}O & ^{1}H	e CC
$\bar{\nu}_e$	CC	0.5-100 GeV	^{16}O & ^{1}H	anti e CC
ν_e	NC	0.5-100 GeV	^{16}O & ^{1}H	e NC
$\bar{\nu}_e$	NC	0.5-100 GeV	^{16}O & ^{1}H	anti e NC
ν_μ	CC	0.5-100 GeV	^{16}O & ^{1}H	μ CC
$\bar{\nu}_\mu$	CC	0.5-100 GeV	^{16}O & ^{1}H	anti μ CC
ν_μ	NC	0.5-100 GeV	^{16}O & ^{1}H	μ NC
$\bar{\nu}_\mu$	NC	0.5-100 GeV	^{16}O & ^{1}H	anti μ NC
ν_τ	CC	0.5-100 GeV	^{16}O & ^{1}H	τ CC
$\bar{\nu}_\tau$	CC	0.5-100 GeV	^{16}O & ^{1}H	anti τ CC
ν_τ	NC	0.5-100 GeV	^{16}O & ^{1}H	τ NC
$\bar{\nu}_\tau$	NC	0.5-100 GeV	^{16}O & ^{1}H	anti τ NC

Table 3.3: Overview of the GiBUU data used in this work

3.2 Parameter Overview

In the following section, the parameters that were analysed during this work will be presented. The physical meaning of the parameters will shortly be outlined and possible special aspects of the calculation will be highlighted. Theses parameters can be used to characterize the simulation behavior of a (neutrino) interaction event generator and gives us the possibility to analyse the performance of GiBUU/KM3BUU compared to GENIE/gSeaGen.

3.2.1 Energy of the Incoming Neutrino E_ν

The energy of the incoming neutrino E_ν is specified during the generation of the neutrino interaction. For GiBUU the runs were created with the energy following a power law, meaning it follows a $1/e$-distribution of the amount of events generated with a certain energy. For each event the interaction particles are stored with their respective energy, momentum and other characteristic parameters that can be extracted from the gSeaGen or KM3BUU data.

3.2.2 Energy of the Outgoing Lepton E_{LepOut}

The energy of the outgoing lepton E_{LepOut} specifies the energy of the lepton leaving the neutrino-nucleus interaction and is therefore calculated by the respective event generator GENIE or GiBUU. In the CC interactions the outgoing lepton is a charged lepton of the same family as the incoming neutrino (so for example an electron in the case of an initial electron neutrino. In NC interactions the neutrino only transfers energy and therefore the lepton leaving the interaction is still a neutrino of the same flavor as the incoming neutrino.

3.2.3 Event Weighting w_2

The weight w_2 is s calculated by gSeaGen or KM3BUU and assigns each interaction event a certain weight value, which can be used to modify the present neutrino energy spectrum. This allows the

generation of spectra in ways they are for example expected from atmospheric neutrinos that have traversed earth and are now interacting with nuclei in the detector volume. Also this enables the study of transport mechanisms and other effects influencing the composition of the neutrinos arriving at the detector. In our case of comparing two different neutrino event generators, this gives us the possibility to scale both or one of the data sets in order to account for different neutrino flux spectra and to make them adequately comparable.

3.2.4 Bjorken-X x_b

The bjorken-x scaling parameter is given as:

$$x_b := \frac{Q^2}{2Pq} = \frac{Q^2}{2M\nu} \tag{3.1}$$

Q is a parameter regarding the four-momentum transfer of a nuclear interaction. It is defined as $Q^2 = -q^2 = -(p - p')^2$ with p being the four-momentum of the incoming particle and p' the four-momentum of the lepton leaving the interaction. The respective particle is the same as the one which is looked at when then energy of the outgoing lepton is defined. P is the four-momentum of the nucleus or nucleon involved in the interaction. ν is a Lorentz-invariant value, that is defined as follows:

$$\nu := \frac{Pq}{M} \tag{3.2}$$

With the nucleon-mass M. In the labframe of this nucleon P is given as $P = (Mc, \vec{0})$ and $q = ((E - E')/c\vec{q})$ where $\vec{q} = \vec{p} - \vec{p'}$. When looking at high energy collision with nucleons with very short reaction times and $Q^2 \gg M^2c^2$, one can approximate that $\nu = E - E'$, which leads to the definition in equation 3.1 (Povh et al., 2014). Within this approximation, this allows to describe the scattering of a high energetic particle on a nucleon in a way that it only depends on one variable, the bjorken-x.

3.2.5 Bjorken-Y y_b

Another important dimensionless and Lorentz-invariant variable is the so called bjorken-y or elasticity, that describes the percentage of the incoming particle's energy that is transferred to the nucleon. It is defined as follows (Formaggio and Zeller, 2012):

$$y_b := \frac{P \cdot q}{P \cdot p} \tag{3.3}$$

Again, P is the four-momentum of the target, $q = |\vec{q}|$ the four-momentum transfer and p the four-momentum of the incoming particle, so in our case the neutrino. In the labframe of the target particle and with several assumptions, the elasticity can be simplified to:

$$y_b = 1 - \frac{E'}{E} \tag{3.4}$$

With E and E' being again the energies of the incoming and outcoming lepton. We will reffer to this version of the bjorken-y as the so called *simplified bjorken-y*. The bjorken-y parameter can be used in a similar way as the bjorken-x, for parameterizing the equation describing the scattering process of a particle interaction. In the context of neutrino event generators, this parameter and

especially the comparison of the true value obtained with equation 3.3 and the simplified value according to equation 3.4 allows the analysis of the generator and especially the comparison to other generators, since this shows the connection between various important output values of the interaction simulation.

3.2.6 Scattering Angle $\theta_{\nu,l}$

The scattering angle describes how the outcoming lepton's direction of movement is altered through the interaction with respect to the initial particle's propagation. It is calculated as follows using the direction $\vec{x}_\nu$ of the incoming neutrino and $\vec{x}_l$ of the outgoing lepton:

$$\theta_{\nu,l} = \arccos \frac{\vec{x}_\nu \cdot \vec{x}_l}{|\vec{x}_\nu||\vec{x}_l|} \tag{3.5}$$

The scattering angle is like x_b and y_b an important parameter in the description of a scattering process.

3.2.7 Total Cross Section σ_{tot}

The total cross section σ_{tot} defines the scattering cross section that has been calculated for a certain interaction as a sum of the different cross sections models. The modelling of the cross section in this way in order to describe different scattering mechanisms for a given neutrino energy is the go to approach for simulating particle interactions, as described in section 2.3. In the case of GiBUU the cross section σ_{tot} is defined as the sum of the elastic and inelastic scattering cross section σ_{QE}, the resonance scattering cross section σ_{RS}, the deep-inelastic scattering cross section σ_{DIS} and the cross section due to background processes σ_{BG} (Lalakulich, 2011).

$$\sigma_{tot} = \sigma_{QE} + \sigma_{RS} + \sigma_{DIS} + \sigma_{BG} \tag{3.6}$$

GENIE uses the same approach for modelling the cross section (Andreopoulos et al., 2010). As highlighted in section 2.3, it is very important to avoid double counting of interactions due to different energy specific models, especially in the transit regions between the validity of these models.

4 Results

In the following chapter, we will go through the procedure of the data analysis and the evaluation of the current implementation of the GiBUU event generator in the KM3NeT simulation with the KM3BUU software package. In the first steps the general neutrino flux spectrum will be compared to the currently implemented gSeaGen package and the application of the weights in order to create comparable spectra is shown. Afterwards the previously presented parameters will be analysed and compared to the ones extracted from gSeaGen data. For each analysis step the results will be presented and interpreted. In the last chapter a conclusion of the obtained results and insights regarding the usage of GiBUU for the KM3NeT neutrino telescope and the evaluation of neutrino events generators will follow.

The data mainly used for the comparison of the behaviour of the different neutrino generators are - if not specified otherwise - combined data sets of anti muon CC and muon CC runs. For GiBUU this provided a set of 1,137,032 events, for gSeaGen 9,565,800 events were included. The normalization of the analysed parameter distributions ensures the comparability independent of the number of included events. Nevertheless, one can clearly see that the gSeaGen distributions show a smoother behaviour due to the data set being nearly 9 times as big.

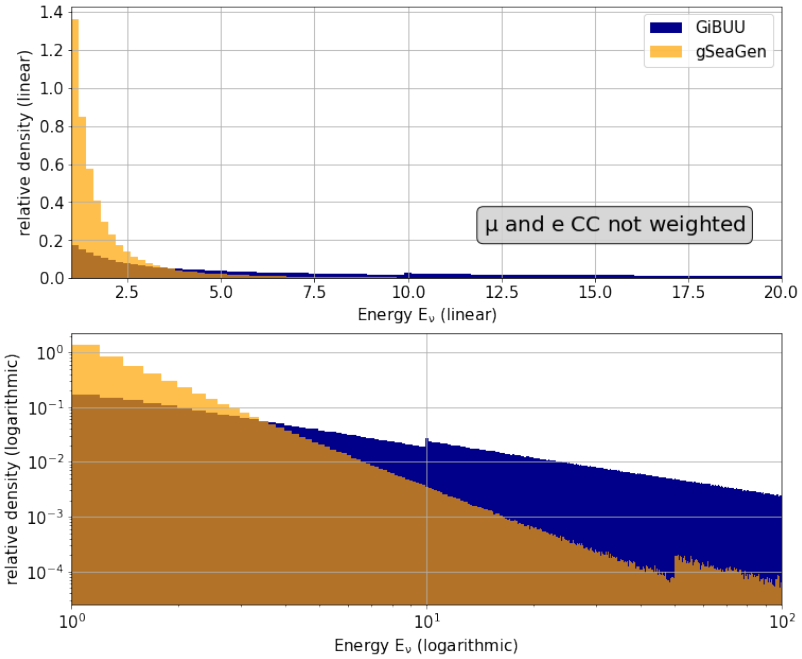

Figure 4.1: Normalized **unweighted** energy distribution of ν_e and ν_μ CC interactions for KM3BUU *(blue)* and gSeaGen *(orange)*. *Upper figure*: Energy range 1 - 20 GeV both axis linear, *Lower figure*: Energy range 1 - 100 GeV both axis logarithmic

4.1 Energy Distribution and Weighting

When comparing two data sets from neutrino event generators, the first step is to examine the energy spectra of the incoming neutrino flux. In order to be able to make valid comparisons of the generated events and their appearance in the context of the entirety of generated events, both fluxes have to be aligned, which is most easily achieved by modifying the flux output of one generator with respect to the other. This requires knowledge about the configuration of both generators. For the data under consideration that is described in section 3.1 , we will modify the GiBUU data with regard to the gSeaGen data by applying certain weights for each event that is generated with the KM3BUU package and assigns each type of event a respective "importance" or probability of appearance. For the events generated with GENIE, gSeaGen assigns weights in the same way and a modification in the reverse direction, meaning the alignment of gSeaGen data with KM3BUU data, or the respective weighting of both data sets would have also been possible.

We will first have a look at the energy distribution of the unweighted data. For the purpose of visualisation the combination of muon neutrino ν_μ and electron neutrino ν_e CC interaction is chosen, since this represents the biggest match of interactions that are available from both KM3BUU and gSeaGen runs. In figure 4.1 on page 34 you can see the normalized energy spectrum for both data sets. In the upper plot, the distributions are shown for energies from 1 to 20 GeV with linear x- and y-axis. The restriction to this energy-range in the upper image is made for better visibility of the distribution, since a lot more events with low energies are generated in both data sets. In the lower plot, both axis are in logarithmic scale and the complete energy range of 1 to 100 GeV is included.

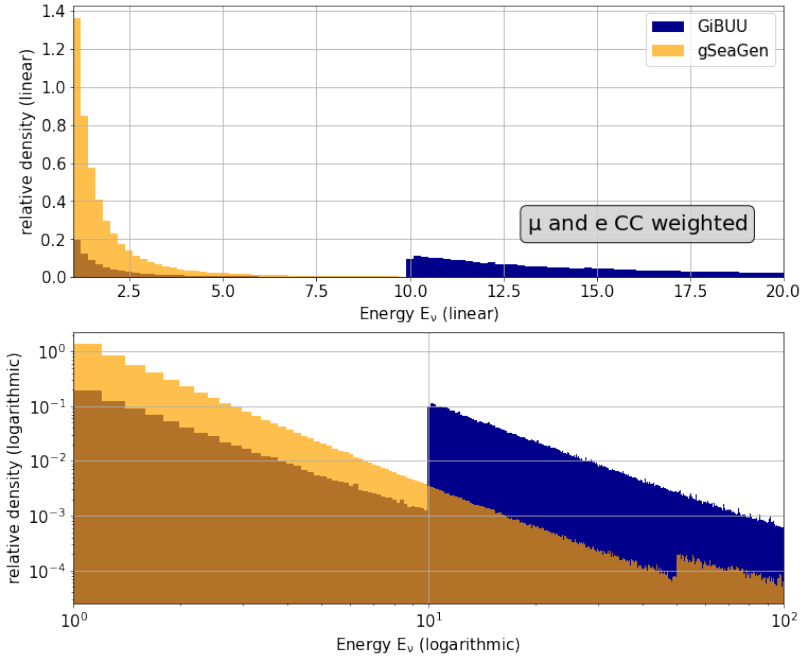

Figure 4.2: Normalized **weighted** energy distribution of ν_e and ν_μ CC interactions for KM3BUU *(blue)* and gSeaGen *(orange)*. *Upper figure*: Energy range 1 - 20 GeV both axis linear, *Lower figure*: Energy range 1 - 100 GeV both axis logarithmic

As you can see from the lower image, both energy spectra are following a power law for certain energy sections, well seen in the section wise linear progression of the logarithmic histograms. However, the two energy distributions differ very much and one could expect the effects arising from this deviation of the energy spectra to severely dominate the differences between both data sets. This is why in the further analysis certain weights are applied to the GiBUU events to account for the different energy distribution. The assigned weights are stored with each event and can be applied during the calculation of the event density distribution for the respective analysis. In figure 4.2 both distributions are shown again, this time with the presentation of the GiBUU data being modified in the respective way.

A distinctive feature that can still be seen in the weighted GiBUU plot, especially in the logarithmic presentation are the steps in the energy distribution at 10 GeV in the GiBUU data and at 50 GeV in the gSeaGen data. As mentioned in sections 3.1.1 and 3.1.2, the gSeaGen and GiBUU data sets of muon CC interactions are each present in a lower and higher energy data set, with the border energy being 10 GeV for the GiBUU data and 50 GeV for gSeaGen. The origin of this feature could not yet be identified, but even though it is very likely due to an error in the data combination process and weight application in the author's code, a further investigation into the weight calculation in the use of combined energy range data is suggested in order to rule out a potential error.

For assuring the comparability of both data sets, the energy range is reduced to 1 to 10 GeV for the further analysis in order to provide a comparable data basis. In figure 4.3 the energy spectra for gSeaGen and unweighted and weighted GiBUU data is shown. As one can see both data sets can be treated as if the same neutrino flux has been provided by both generators in this way.

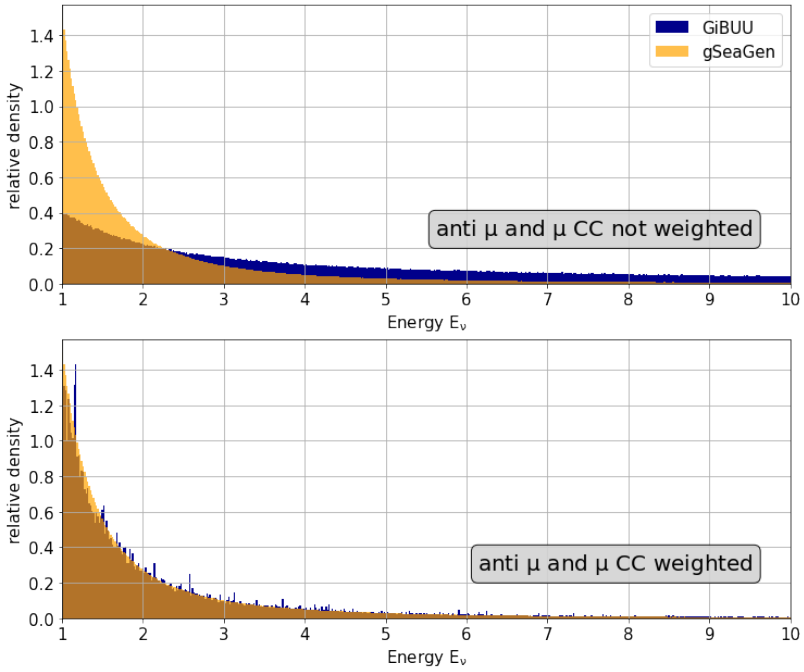

Figure 4.3: Normalized energy distribution of $\bar{\nu}_\mu$ and ν_μ CC interactions for KM3BUU *(blue)* and gSeaGen *(orange)* in the energy range of 1 to 10 GeV. *Upper figure*: No weighting applied, *Lower figure*: Weighting applied

The alignment of the GiBUU data with the gSeaGen data is done using the following weighting, which includes the weights calculated by KM3BUU w_2, the number of events in each run N_{events} and the neutrino energy of each event E_ν:

$$w = \frac{w_2}{N_{events}} \cdot E_\nu^{-1.4} \tag{4.1}$$

This weight will be applied to all the GiBUU data that has been converted to the KM3NeT dataformat, so a side by side comparison between the data from GiBUU and gSeaGen is possible.

4.2 Bjorken-Y

In this section the distribution of the bjorken-y parameter will be examined in different ways in order to compare both generators and their implementations. We will first have a look at the data provided by GiBUU without further KM3NeT-specific data rearrangement or modification, as it is obtained using the GiBUUOutput function from the km3buu.output package and then examine how the respective data is present after being modified for KM3NeT usage. In this case, the data is obtained using the function OfflineReader from the km3io package, as it is also done with the gSeaGen data.

4.2.1 GiBUU Output

In this section the data received using the GiBUUOutput function will be analysed with regard to its distribution of generated particle and interaction types. When available, the gSeaGen data is analysed in the same way and a comparison is given. Since the data of both generators shows respectively the same "behaviour" of the distributions of certain data each for both muon and electron runs and there is no big loss of information due to the restriction to one of the two flavor cases, the further analysis will focus on muon CC runs when comparing GiBUU and gSeaGen. Notice that no KM3BUU weights for the GiBUUOutput events were available for the use in this analysis, so a direct comparison of the distribtuions with the ones from gSeaGen are not possible. However, since we are not interested in a quantitative comparability of both data sets we can have a look at the whole energy range from 1 to 100 GeV.

In figure 4.4 you can see the distribution of the true bjorken-y over the simplified bjorken-y on the left and the difference between both being plotted over the neutrino energy on the right for muon CC runs generated by GiBUU.

You can see that both parameters tend to agree better in higher neutrino energies and when the calculated bjorken-y approaches its limit values of 0 or 1. For most cases both parameters agree very well with the deviation being present in only few runs (notice the logarithmic colorbar!). For comparison, in figure 4.5 the corresponding gSeaGen data is shown in the same way.

The overall behaviour in both event generators is the same, with the gSeaGen data showing a wider spread between both parameters. However, the comparability of both generators is not really given here, since this is the unweighted data in which the energy spectrum of the gSeaGen data is way more concentrated on lower energies with respect to GiBUU, as you can see from figure 4.1. Since the general agreement between both bjorken-y parameters is better in high energy processes, the slightly different wider spread in the gSeaGen plot can be traced back to the different flux spectrum.

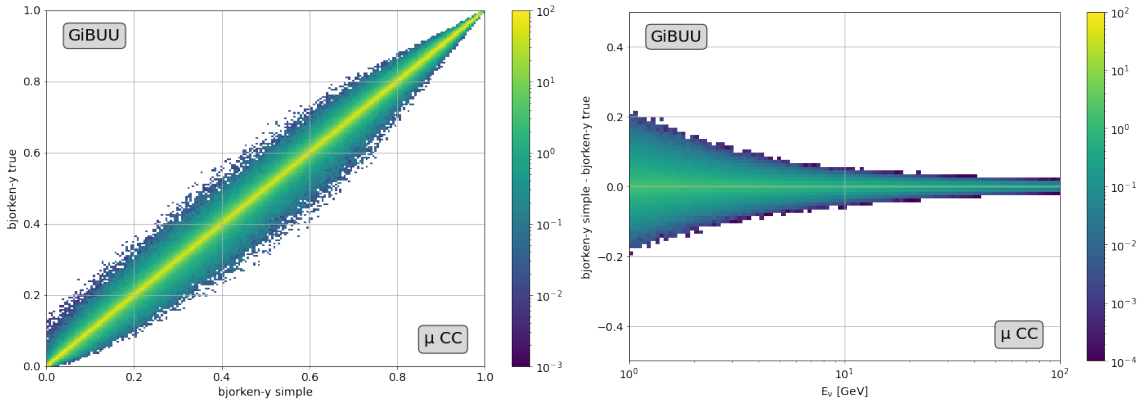

Figure 4.4: Distribution of bjorken-y and simplified bjorken-y for GiBUU muon CC runs (GiBUU Output)

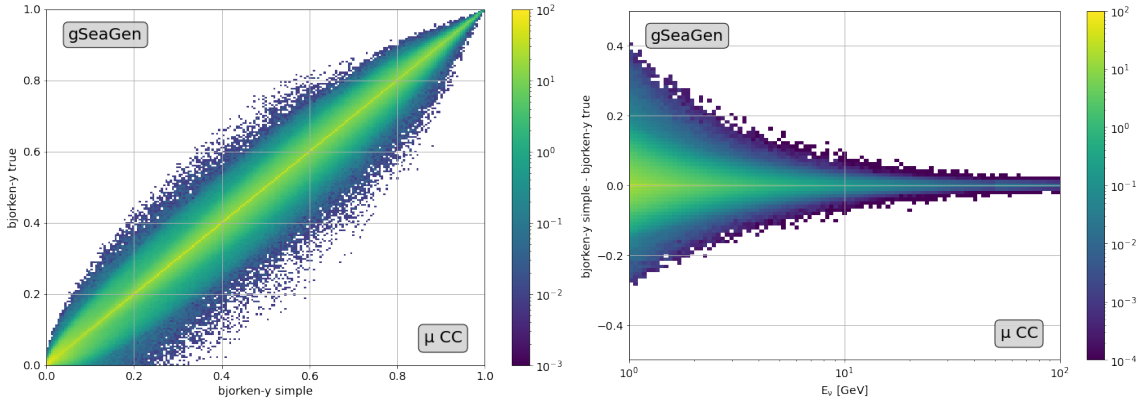

Figure 4.5: Distribution of bjorken-y and simplified bjorken-y for gSeaGen muon CC runs

Even though the data is present with two different spectra, we can have a look at internal differences between generated event types for both generators and compare the results. Therefore, the same histograms are created for anti muon CC runs and the difference between the anti muon CC and the muon CC distribution is presented. You can see the respective plots in figure 4.6 for GiBUU and 4.7 for gSeaGen data.

A remarkable difference between GiBUU and gSeaGen data can be observed. For GiBUU both anti muon and muon CC runs are very similarly distributed when looking at the bjorken-y parameter. The differences are therefore very low and are homogeneously spread over the range of the data. It seems that the anti muon CC runs have a slightly better agreement of the bjorken-y parameters, as one can see from the accumulation of blue points along the diagonal line in the left plot. The distribution over the energy also shows only small differences and a slight excess of anti muon CC runs in the higher energies. Since this is the region where the approximations for the simplified bjorken-y are more valid, this explains the seemingly better agreement of both parameters in the left plot.

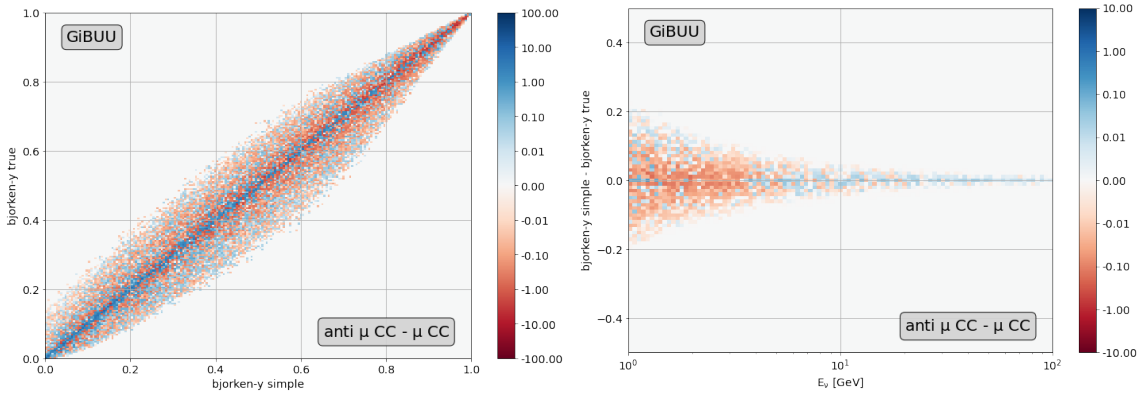

Figure 4.6: Difference in bjorken-y and simplified bjorken-y between GiBUU anti muon CC and muon CC runs (GiBUU Output)

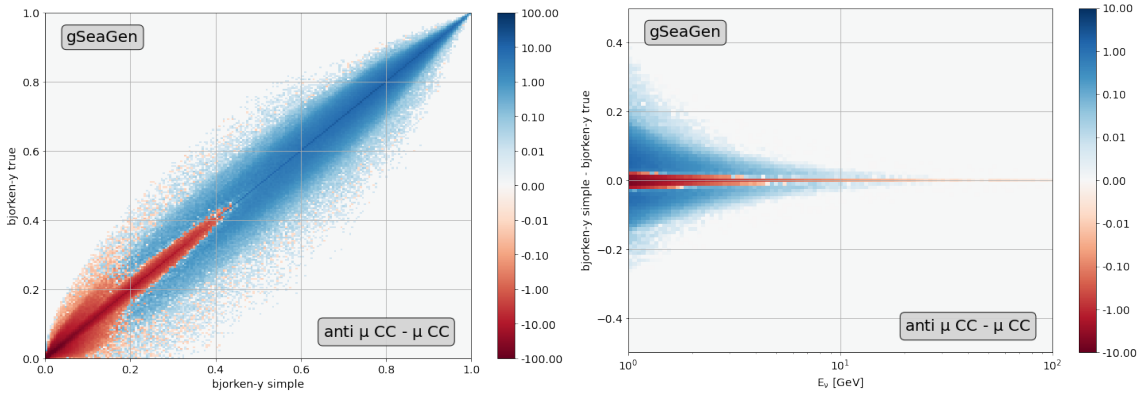

Figure 4.7: Difference in bjorken-y and simplified bjorken-y between gSeaGen anti muon CC and muon CC runs

The gSeaGen data on the other hand shows a strong difference between anti muon CC and muon CC runs. There are regions in which the density of the muon runs is much higher compared to the anti muon runs. One can see, that more muon events with lower bjorken-y are generated and that these events show a better agreement of both parameters over the whole energy range. This treatment shows a strong difference between both generators and a further investigation about the origin of this difference is suggested. For better comparability a similar distribution for all event types would be desirable in both data sets.

In figure 4.8 the difference between muon CC and muon NC runs for GiBUU data is shown. Unfortunately the available gSeaGen NC data had some issues, which disabled to create a comparable analysis with it. This is why only the GiBUU results are shortly presented.

From the plots one can conclude that the generated NC events seem to have a better agreement of both parameters and are slightly more present in higher energies, which is probably also the reason for the better agreement of both bjorken-y, comparably to the anti muon - muon difference in figure 4.6.

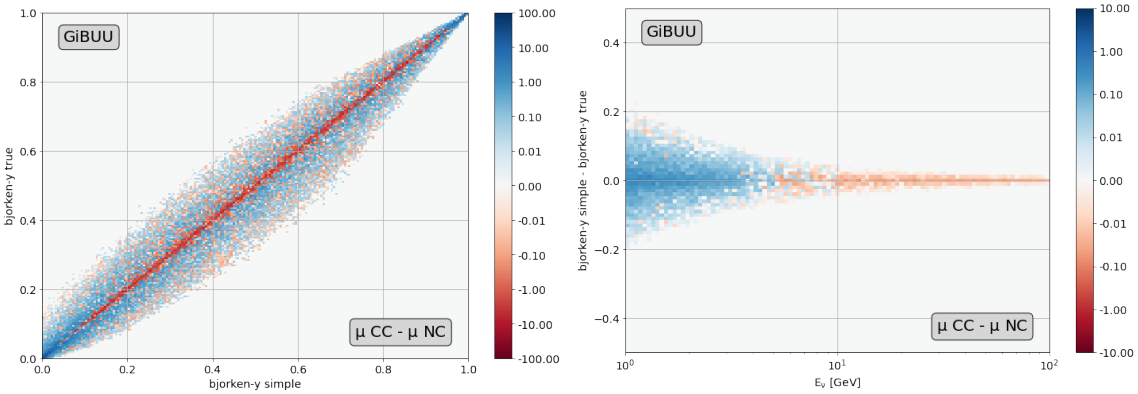

Figure 4.8: Difference in bjorken-y and simplified bjorken-y between GiBUU muon CC and muon NC runs (GiBUU Output)

4.2.2 KM3BUU Output

We will now have a look at the data sets that were already modified by KM3BUU and converted into the GiBUU data into the KM3NeT data format. These data sets are designed to be obtainable in the same way as the gSeaGen files, by using the OfflineReader function from the KM3IO package, that is generally used in the analysis of data from KM3NeT. Notice that the respective weights as defined in equation 4.1 are applied to the GiBUU data. For figures 4.9 and 4.10 the same analysis regarding the bjorken-y parameter will be done as described in the previous section. This time only the energy range from 1 to 10 GeV was selected, which in combination with the weighting and the normalization of the histograms should allow a direct comparison between both data sets.

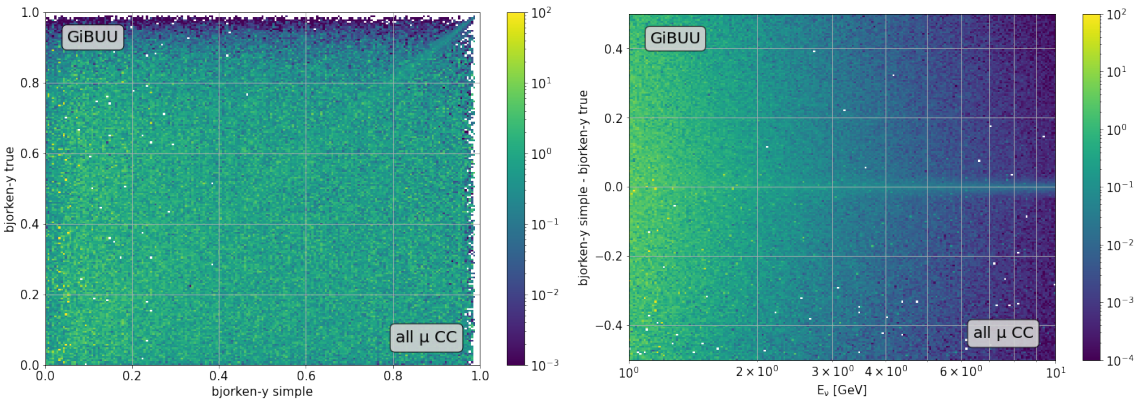

Figure 4.9: Distribution of bjorken-y and simplified bjorken-y for GiBUU anti muon CC and muon CC runs (KM3BUU Output)

One can clearly see that there is a problem with the GiBUU data here. Even though one can see the hint of a diagonal line in the left plot and a horizontal line at zero difference in the right plot of figure 4.10, the general distribution is very random and both bjorken-y parameters don't seem to follow a distinctive connection. This is either due to a bug in the code for generating the GiBUU runs with

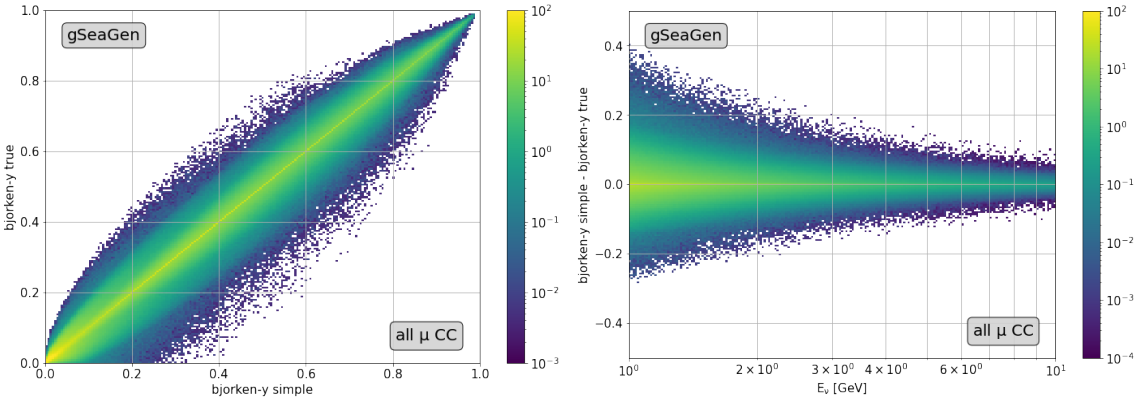

Figure 4.10: Distribution of bjorken-y and simplified bjorken-y for gSeaGen anti muon CC and muon CC runs

KM3BUU, so they are present in the KM3NeT format, or in the author's code when loading and connecting the data.

We will therefore have a closer look at the differences that occur with the same data being present as GiBUU output on one hand and as KM3BUU output on the other hand. For the sake of demonstration the muon CC runs with oxygen as target material are chosen and the assigned bjorken-y value of each event will be extracted together with the energy of the incoming neutrino and the outgoing lepton, so in this case the muon leaving the interaction. This allows the calculation of the simplified bjorken-y, what can be used for characterizing both data sets and to analyse potential differences in the treatment of the data. In figure 4.11 the distribution of the true bjorken-y value that is calculated in the event generator is shown. The modified data being present in the KM3NeT dataformat is shown in orange and labelled "OfflineReader" after the function that is used to load the data. The data provided directly by GiBUU, that is loaded with the GiBUUOutput function is shown in blue and labeled respectively.

One can see that the distribution is slightly altered through the conversion into KM3NeT data format but overall still shows the same shape as the original GiBUU data. In figure 4.12 the same plot is shown for the respective simplified bjorken-y parameters. For both data sets, it gets calculated using equation 3.4 ($y_b = 1 - E'/E$), using the energy of the incoming muon neutrino ($E = E_\nu$) and the outgoing muon ($E' = E_\mu$).

Figure 4.12 shows that the distribution of the calculated simple bjorken-y differs between both data sets. The distribution of the KM3BUU data shows a better agreement with the true bjorken-y distribution as one can see from comparison with figure 4.11. However, the distribution of the GiBUU simple bjorken-y shows a different shape compared to the other ones, having a slight excess in higher bjorken-y and less events with lower bjorken-y compared to the KM3BUU one. Both bjorken-y parameters are plotted against each other, which is shown in figure 4.13 for both data sets. Notice, that this is only a small fraction of the previously analysed data, since this simplified the analysis of the code used for the calculation of the simple bjorken-y and still allows for a comparison of both data formats. Also, no weights were applied for these plots.

The data available in the KM3NeT data format shows again an unexpected distribution of bjorken-y parameters. This indicates a problem, during either the assignment of values when rearranging the

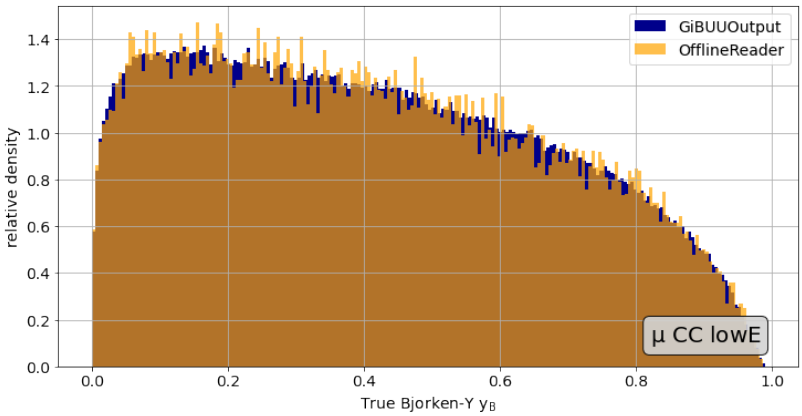

Figure 4.11: Distribution of the true bjorken-y parameter for one muon CC data set that was given as direct output from GiBUU ("GiBUUOutput") and after transformation into KM3NeT format with KM3BUU ("OfflineReader")

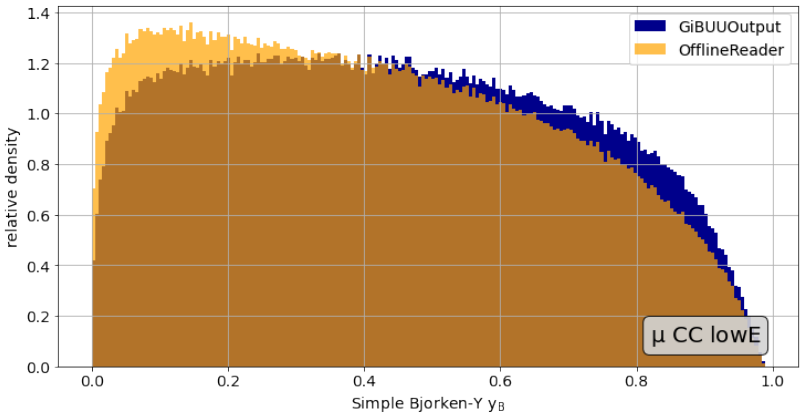

Figure 4.12: Distribution of the simple bjorken-y parameter for one muon CC data set that was given as direct output from GiBUU ("GiBUUOutput") and after transformation into KM3NeT format with KM3BUU ("OfflineReader")

data from GiBUU to KM3NeT format or in the extraction of incoming and outgoing lepton energies. For clarification, in the following plot the true bjorken-y value is plotted over the obtained energy of the outgoing lepton. The GiBUUOutput data shows a linear dependency of the true bjorken-y regarding the energy of the outgoing lepton, which makes sense in a way that the data has events with initial neutrino energies from 0.5 to 10 GeV and a high bjorken-y means that a little part of the energy is carried away by the lepton and the other way around for a high bjorken-y. The OfflineReader data on the other hand shows a more or less random distribution of the bjorken-y values over the energy, which does not go along with the expected property. The vertical line symbolises the minimal energy of the incoming neutrinos.

This shows that most probably the error lies in the extraction of the energy of the outgoing lepton, since on one hand the expected linear dependency is not present and on the other hand there

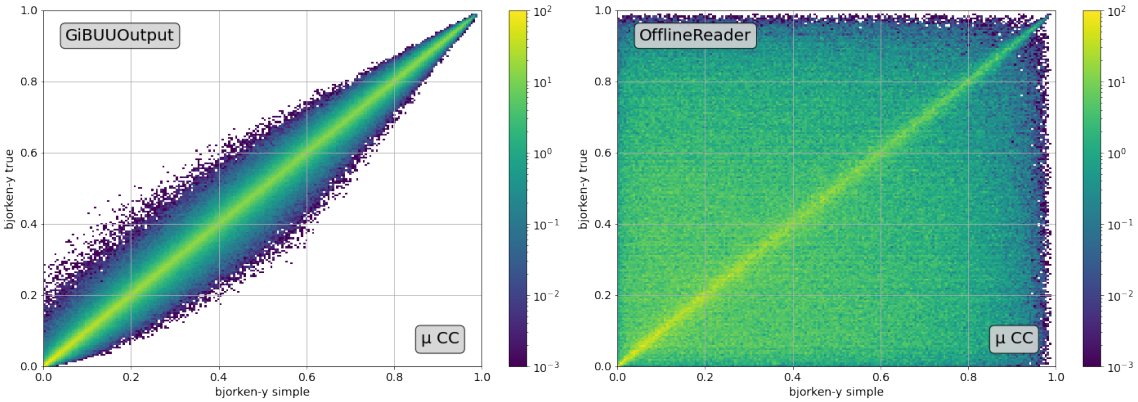

Figure 4.13: Distribution of bjorken-y and simplified bjorken-y for muon CC runs in GiBUU data *(left)* and KM3NeT format *(right)*)

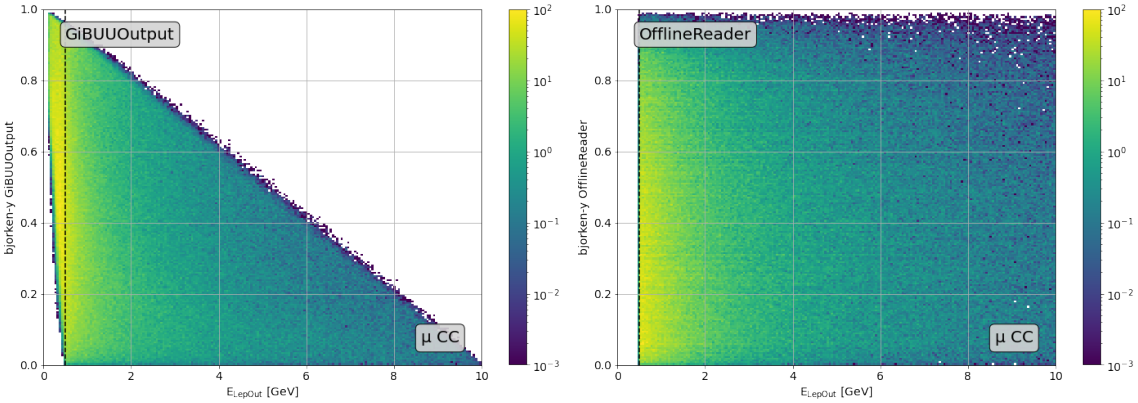

Figure 4.14: Distribution of true bjorken-y over the energy of the outgoing lepton for muon CC runs in GiBUU data *(left)* and KM3NeT format *(right)*)

are no outgoing lepton energies below 0.5 GeV, which would be expected for very high bjorken-y processes. Another problem could be the internal assignment of the true bjorken-y to each event, with a possible mismatch between the event from which the bjorken-y is calculated in GiBUU and the event to which this bjorken-y is assigned to in the KM3BUU data.

Since the same code applied on the gSeaGen data works and gives the expected results, a difference regarding the particle's energies is present between the gSeaGen and the KM3BUU files which are originally meant to have the same data structure, so the GiBUU generator can be used inside the KM3NeT chain. It is recommended that this is further analysed in the KM3BUU code in order to avoid potential problems in the future.

4.3 Energy of the Outgoing Lepton

In this section we will have a look at the outgoing lepton's energy, to which we will refer to as "ELepOut" in the following. We will both have a look at the distributions of ELepOut over the neutrino energy and at the difference between both energies over the neutrino energy. We will again use the weighted GiBUU data for this analysis and restrict the data to an energy range from 1 to 10 GeV and include a combination of anti muon CC and muon CC runs in order to ensure comparability between both data sets. In figure 4.15 both plots are shown for the GiBUU data set. Figure 4.16 shows the analogue case for the gSeaGen data set.

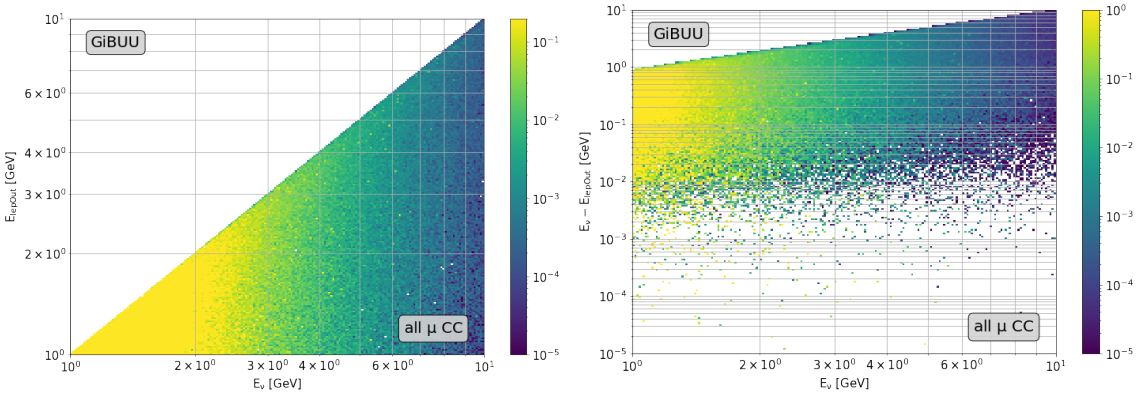

Figure 4.15: Distribution of ELepOut *(left)* and the difference between neutrino energy and ELepOut *(right)* over the energy of the outgoing lepton for muon CC runs in GiBUU

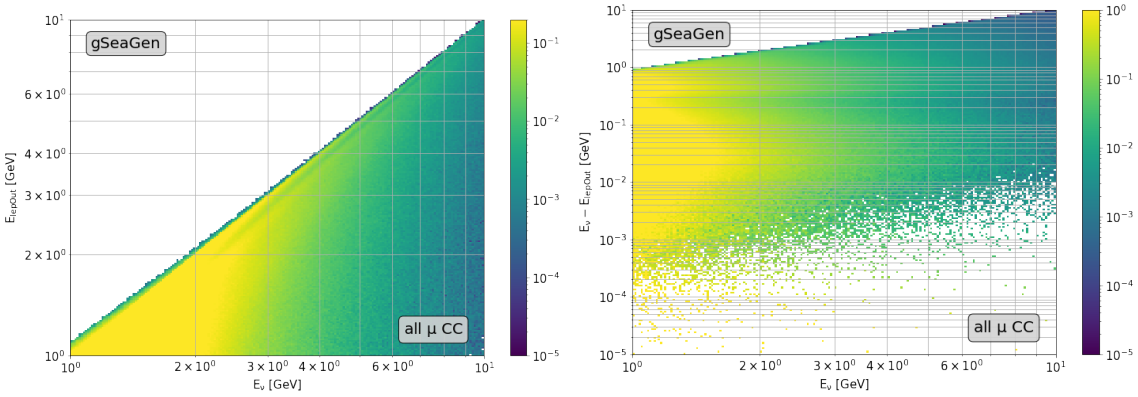

Figure 4.16: Distribution of ELepOut *(left)* and the difference between neutrino energy and ELepOut *(right)* over the energy of the outgoing lepton for muon CC runs in gSeaGen

We see that the distributions from GiBUU and gSeaGen are generally in the same shape for both plots under consideration. Both generators are producing more events with lower energies, as could already be seen in section 4.1. However, the energy of the outgoing lepton never seems to fall below the minimal initial neutrino energy of 0.5 GeV in the GiBUU data. This leads to the strictly diagonal shape of the distribution with a sharp border. In gSeaGen there are also interactions which lead to

outgoing leptons with energies below 0.5 GeV, as it is expected. This indicates again a problem in the assignment or calculation of ELepOut in KM3BUU. In figure 4.17 the difference between the distributions of the respective GiBUU and gSeaGen data is shown.

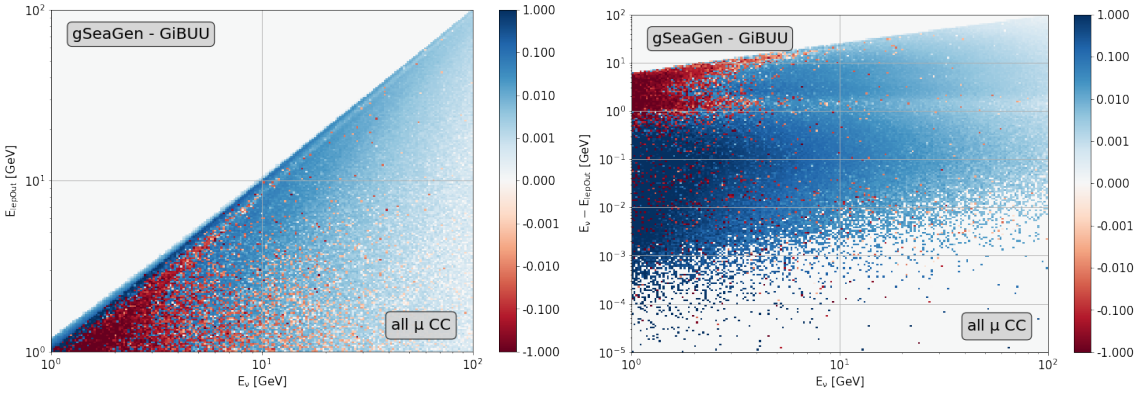

Figure 4.17: Difference between the gSeaGen and GiBUU distributions of ELepOut *(left)* and the difference between neutrino energy and ELepOut *(right)*) over the neutrino energy for muon CC runs

This presentation highlights the difference regarding the simulation of outgoing leptons with energy below the minimal initial neutrino energy. Also, one can see that the general density of the generated interactions is higher in the lower energies for GiBUU data. Furthermore, a certain effect seems to be active in the generation of the gSeaGen data, which causes a visible deviation from the otherwise smoothly distributed energy difference in for energy differences between 1 and 2 GeV that can be observed over the whole energy range. This is most likely caused by a switch in the model composition regarding the simulated interaction processes that contribute to the overall cross section for a certain energy. As presented by Andreopoulos et al., 2010, the transition between two models is done in an energy window between 2.3 and 3.0 GeV, which would explain the sudden change in the observed distributions. One has to keep this in mind when analysing current gSeaGen data in order to be able to explain possible effects arising from this.

4.4 Scattering Angle

In this section the scattering angle and its distribution over the neutrino energy and over the respective true bjorken-y of the event will be analysed for both neutrino generators and the results will be compared.

The distributions in figure 4.18 and 4.19 show a good matching when comparing the data sets from the different neutrino generators. One can see that both data sets include events with scattering angles of up to around 3.15 degrees and all of the possible scattering angles are existent throughout the whole energy range with an overall trend of higher scattering angles at lower neutrino energies. However, one has to keep in mind that more events with lower energies are generated, which is why of course the whole distribution is concentrated at lower energies. For gSeaGen there are more events with low scattering angle present in higher energies when compared to GiBUU.

The presentation of the scattering angle over the true bjorken-y shows a good agreement of the

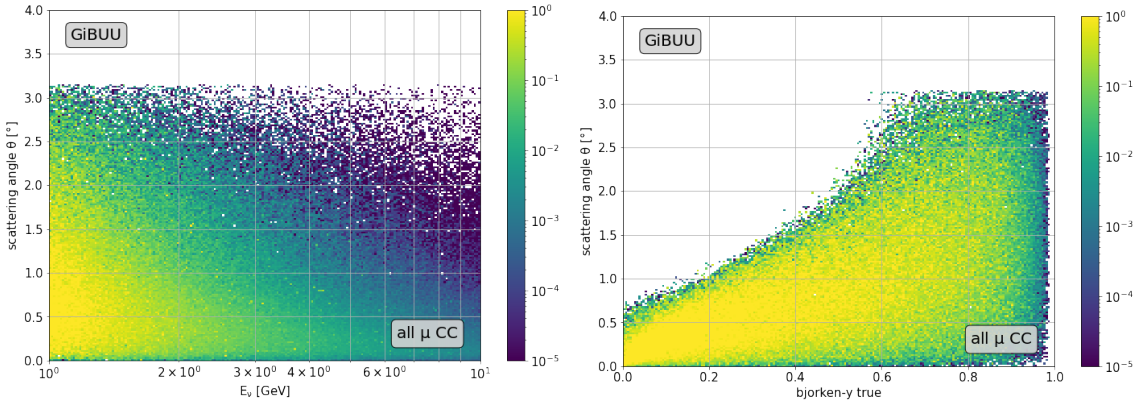

Figure 4.18: Distribution of the scattering angle over the neutrino energy *(left)* and over the true bjorken-y *(right)* for muon CC runs in GiBUU

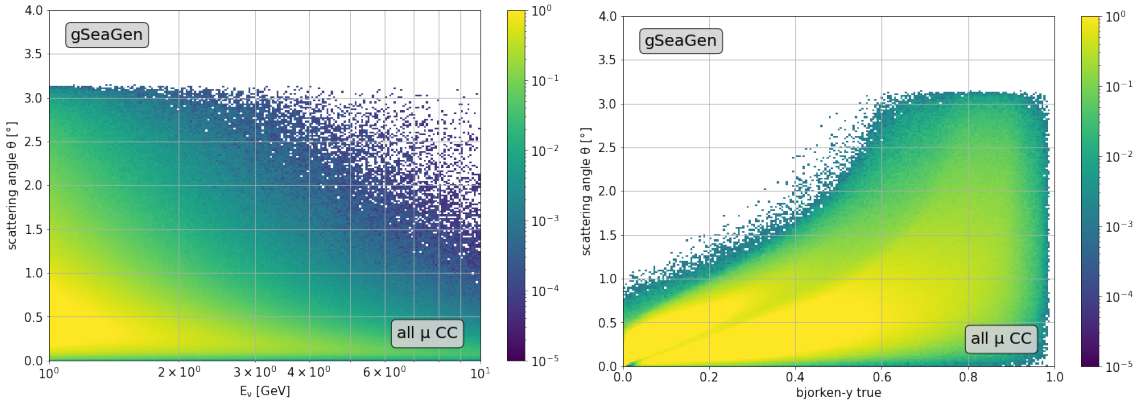

Figure 4.19: Distribution of the scattering angle over the neutrino energy *(left)* and over the true bjorken-y *(right)* for muon CC runs in gSeaGen

distributions from the different event generators as well. In both cases higher scattering angles are connected with a high bjorken-y and therefore a high energy transfer from the neutrino to the nucleon, which is expected. However there is again an effect visible in the gSeaGen distribution that disrupts the otherwise smooth distribution. It is remarkable, that this can only be seen in the plot over the bjorken-y and not in the distribution over the energy. The previously mention artefact in the gSeaGen distribution over the scattering angle is well visible in the difference plot in figure 4.20 as well. Also, the higher rate of low scattering angle events at higher energies in gSeaGen can clearly be seen in the left plot. Like in the previous chapter, this effect should be kept in mind especially when comparing the performances of different generators for the KM3NeT simultaion chain.

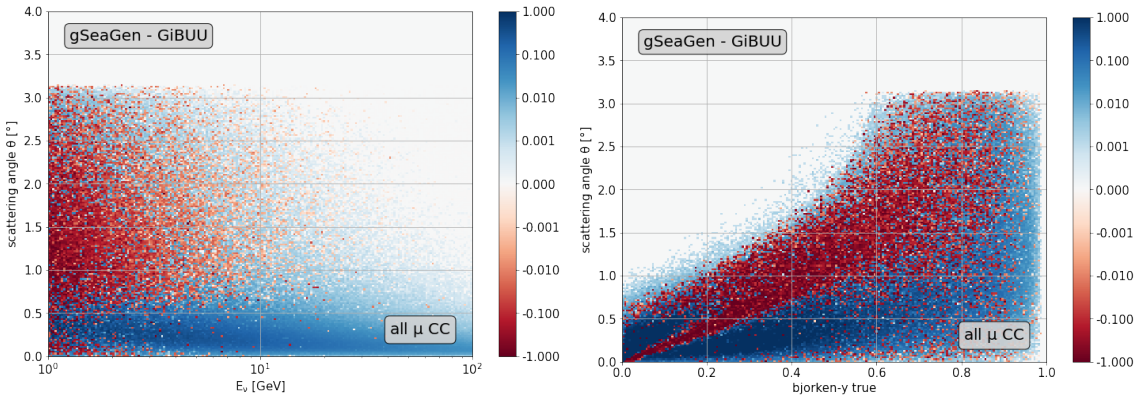

Figure 4.20: Difference between the gSeaGen and GiBUU distributions of the scattering angle over the neutrino energy *(left)* and over the true bjorken-y *(right)* for muon CC runs

4.5 Cross Section

As last analysis point we will have a look at the distribution of the total cross sections for both event generators. For each event the cross section that has been calculated by the respective event generator is saved. In figure 4.21 the relative distribution of both data sets is shown with cross sections up to $1000 \times 10^{-38}\,\mathrm{cm}^2$ being included.

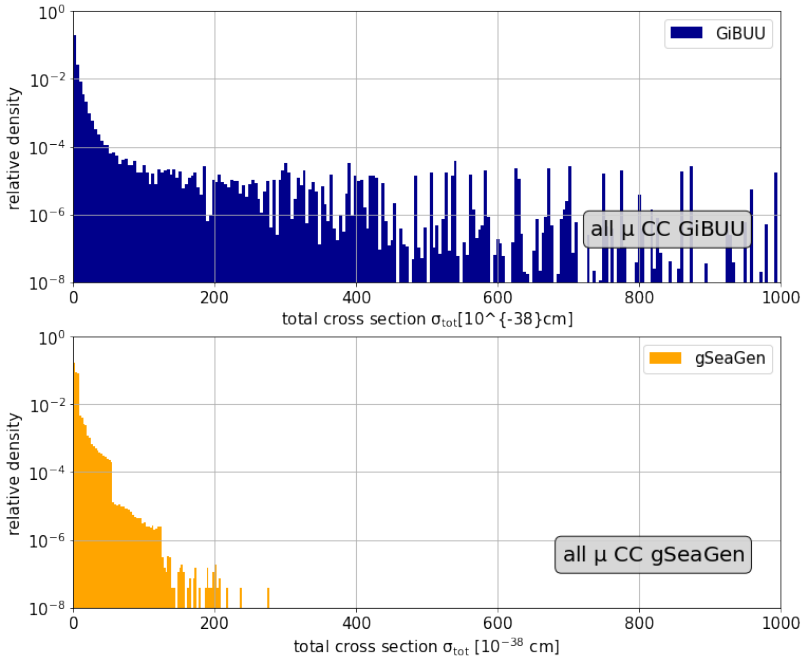

Figure 4.21: Distribution of the total cross section for GiBUU *(upper figure)* and gSeaGen *(lower figure)* for anti muon CC and muon CC runs

Again, the data consists of anti muon CC and muon CC runs with the respective weights being applied to the GiBUU data.

A clear difference between both generators can be seen even though the weighting accounts for an aligned energy spectrum for both data sets. The GiBUU data shows a wider spread over the cross section range whereas the gSeaGen data shows a higher concentration of lower cross sections. This indicates a clear difference in the underlying cross section calculation methods, that has to be considered in the usage and comparison of both generators in the KM3NeT chain.

Another important feature are the steps in the gSeaGen distribution at around 50 and 140 $\times$ $10^{-38}\,\mathrm{cm}^2$. It is suggested to investigate the gSeaGen data regarding systematic uncertainties in the KM3NeT simulation chain arising from this effect in the data. Also the inclusion of KM3BUU into the simultaion chain and the evaluation of its performance by comparing it to the gSeaGen chain and the usage of combined data sets should be treated with respect regarding possible special features originating from this effect.

5 Conclusion and Outlook

In the previous chapter a number of parameters characterizing the data sets generated with GiBUU and gSeaGen were analysed and their respective distributions in both data sets compared. This provided insights into the current state of the inclusion of GiBUU in the KM3NeT analysis chain with the KM3BUU package and the general process of comparing data from different event generators.

First of all, when combining more data sets from different generated runs, one has to mind the different calculation of the respective event weights in the various data sets. To ensure a comparable analysis of different generators the data has to be scaled accordingly, so both sets represent the same incoming neutrino flux. Due to the problems that were present when combining different KM3BUU runs, it is suggested to clarify the origin of these problems and reevaluate the weight calculation for multiple data sets in order to enable a straightforward comparison of event generators in the future.

The analysis of the bjorken-y parameter distribution showed a major difference between both generators regarding the varying properties of particle and anti particle runs. The GiBUU data showed a more or less equal distribution of true and simplified bjorken-y parameter. gSeaGen on the other hand showed strong differences between both cases hinting at a clear difference in the generation process between gSeaGen and GiBUU. A further look into the implications of these differences is suggested.

In addition to the differences of the generated events, a problem with the GiBUU data after the conversion into the KM3NeT data format was detected. The problem seems to have its origin in the assignment of either the bjorken-y value or the structure of the stored particle energies of an event. It is recommended to reanalyse the generated GiBUU data before and after the conversion with KM3BUU and to look for the cause of this deviation from the gSeaGen data structure. The analysis of the distribution of the outgoing lepton's energy reinforced this view. Furthermore a number of effects in the gSeaGen data could be observed, that most likely originate in the transition between different cross section simulation models. These effects should be reconsidered regarding possible systematic influences in the KM3NeT chain and the side by side analysis of multiple event generators.

Considering future work with KM3BUU and gSeaGen, this work proposed a number of points that might be worth being reviewed and analysed in order to assure the correct implementation of the GiBUU event generator or other generators in KM3NeT and to avoid possible errors arising from a lack of knowledge about the underlying data.

Bibliography

Adriá n-Martínez, S et al. (2016). "Letter of intent for KM3NeT 2.0". In: *Journal of Physics G: Nuclear and Particle Physics* 43.8, p. 084001. DOI: 10.1088/0954-3899/43/8/084001.

Aiello, S. et al. (2020). "gSeaGen: The KM3NeT GENIE-based code for neutrino telescopes". In: *Computer Physics Communications* 256, p. 107477. DOI: 10.1016/j.cpc.2020.107477.

ALEPH (1992). *Figures of ALEPH Physics Results: Electroweak Physics*. https://aleph.web.cern.ch/aleph_general/reports/figures/ew/index.html. Accessed: 2022-08-04.

Andreopoulos, C. et al. (2010). "The GENIE neutrino Monte Carlo generator". In: *Nuclear Instruments and Methods in Physics Research Section A: Accelerators, Spectrometers, Detectors and Associated Equipment* 614.1, pp. 87–104. DOI: 10.1016/j.nima.2009.12.009.

Athar, M. Sajjad and S. K. Singh (2020). *The Physics of Neutrino Interactions*. Cambridge University Press. DOI: 10.1017/9781108489065.

Bashmakov, Yu A (2015). "Cherenkov radiation: from discovery to RICH". In: *Physics-Uspekhi* 58.5, pp. 467–471. DOI: 10.3367/ufne.0185.201505f.0502. URL: https://doi.org/10.3367/ufne.0185.201505f.0502.

Berger, Christoph (2014). *Elementarteilchenphysik: Von den Grundlagen zu den modernen Experimenten*. Springer Spektrum Berlin, Heidelberg. ISBN: 978-3-642-41753-5. DOI: 10.1007/978-3-642-41753-5.

Demtröder, Wolfgang (2017). *Experimentalphysik 4: Kern-, Teilchen- und Astrophysik*. 4th ed. Springer Berlin, Heidelberg. ISBN: 978-3-642-21476-9. DOI: 10.1007/978-3-642-21476-9. URL: https://link.springer.com/book/10.1007/978-3-642-21476-9.

Ereditato, Antonio (2018). *The State of the Art of Neutrino Physics*. WORLD SCIENTIFIC. DOI: 10.1142/10600. eprint: https://www.worldscientific.com/doi/pdf/10.1142/10600. URL: https://www.worldscientific.com/doi/abs/10.1142/10600.

Formaggio, J. A. and G. P. Zeller (2012). "From eV to EeV: Neutrino cross sections across energy scales". In: *Rev. Mod. Phys.* 84 (3), pp. 1307–1341. DOI: 10.1103/RevModPhys.84.1307. URL: https://link.aps.org/doi/10.1103/RevModPhys.84.1307.

Griffiths, David (2008). *Introduction to Elementary Particles*. Physics textbook. Wiley. ISBN: 9783527618477. URL: https://books.google.de/books?id=Wb9DYrjcoKAC.

Hallmann, Steffen (2021). "Sensitivity to atmospheric tau-neutrino appearance and all-flavour search for neutrinos from the Fermi Bubbles with the deep-sea telescopes KM3NeT/ORCA and ANTARES". PhD thesis. Friedrich-Alexander-Universität Erlangen-Nürnberg.

KM3NeT-Collaboration (2022a). *KM3NeT: Member Institutes*. https://www.km3net.org/wp-content/uploads/2022/05/Cities-and-Sites-of-KM3NeT_220425-scaled.jpg. Accessed: 2022-08-10.

– (2022b). *KM3NeT Research Infrastructure: KM3NeT-Fr*. https://www.km3net.org/research/research-infrastructure/km3net-fr-site/. Accessed: 2022-08-10.

Lalakulich O.; Gallmeister, K.; Mosel U. (2011). *Neutrino nucleus reactions within the GiBUU model*. DOI: 10.48550/ARXIV.1110.0674. URL: https://arxiv.org/abs/1110.0674.

Leitner, Tina J. (2009). "Neutrino-Nucleus Interactions in a Coupled-Channel Hadronic Transport Model". PhD thesis. Justus-Liebig-Universität Gießen.

Mann, Robert (2010). *An Introduction to Particle Physics and the Standard Model*. CRC Press. ISBN: 978-1-4200-8300-2. DOI: 10.1201/9781420083002.

NIST/CODATA (2018). *Fundamental Physical Constants: Weak Mixing Angle*. hhttps://physics.nist.gov/cgi-bin/cuu/Value?sin2th. Accessed: 2022-08-15.

NobelPrize.org (2022). *The Nobel Prize in Physics 1979: Press Release*. https://www.nobelprize.org/prizes/physics/1979/press-release/. Accessed: 2022-08-11.

Oberauer, Lothar and Judith Oberauer (Jan. 2019). *Neutrinophysik: Grundlagen, Experimente und aktuelle Forschung*. ISBN: 978-3-662-59334-9. DOI: 10.1007/978-3-662-59335-6.

Povh, Bogdan et al. (Jan. 2014). *Teilchen und Kerne*. ISBN: 978-3-642-37821-8. DOI: 10.1007/978-3-642-37822-5.

Robinson, M. et al. (2008). *A Simple Introduction to Particle Physics*. DOI: 10.48550/ARXIV.0810.3328. URL: https://arxiv.org/abs/0810.3328.

Schumann, J. and B. Jung (2021). "GiBUU based neutrino interaction simulations in KM3NeT". In: *Journal of Instrumentation* 16.09, p. C09022. DOI: 10.1088/1748-0221/16/09/c09022.

Spiering, Christian (2020). "Neutrino Detectors Under Water and Ice". In: *Particle Physics Reference Library: Volume 2: Detectors for Particles and Radiation*. Ed. by Christian W. Fabjan and Herwig Schopper. Cham: Springer International Publishing, pp. 785–822. ISBN: 978-3-030-35318-6. DOI: 10.1007/978-3-030-35318-6_17. URL: https://doi.org/10.1007/978-3-030-35318-6_17.

Suekane, Fumihiko (Apr. 2015). *Neutrino Oscillations: A practical guide to Basics and Applications*. Vol. 898. ISBN: 978-4-431-55461-5. DOI: 10.1007/978-4-431-55462-2.

Torres-Rincon, Juan M. (2014). "Boltzmann-Uehling-Uhlenbeck Equation". In: *Hadronic Transport Coefficients from Effective Field Theories*. Cham: Springer International Publishing, pp. 33–45. ISBN: 978-3-319-00425-9. DOI: 10.1007/978-3-319-00425-9_2. URL: https://doi.org/10.1007/978-3-319-00425-9_2.

Wikipedia, Creative Commons (2011). *Neutrino Oscillations: Theory, graphically - Three neutrino probabilities*. https://en.wikipedia.org/wiki/Neutrino_oscillation#Three_neutrino_probabilities. Accessed: 2022-08-18.

Winter, Walter (July 2015). "Neutrino mass hierarchy: Theory and phenomenology". In: vol. 1666, p. 120001. DOI: 10.1063/1.4915577.

Woithe, Julia, Gerfried J Wiener, and Frederik F Van der Veken (2017). "Let's have a coffee with the Standard Model of particle physics!" In: *Physics Education* 52.3, p. 034001. DOI: 10.1088/1361-6552/aa5b25. URL: https://doi.org/10.1088/1361-6552/aa5b25.

Zuber, Kai (2020). "Neutrino Physics". In: Taylor Francis. ISBN: 9781351764582, 9781315195612, 9781032242200, 9781138718890. DOI: 10.1201/9781315195612. URL: https://directory.doabooks.org/handle/20.500.12854/79366.

Eigenständigkeitserklärung

Hiermit bestätige ich, dass ich diese Arbeit selbstständig und nur unter Verwendung der angegebenen Hilfsmittel angefertigt habe.

Erlangen den 26.08.2022

Hannes Warnhofer